Global and Planetary Change 208 (2022) 103684

Contents lists available at ScienceDirect

Global and Planetary Change

journal homepage: www.elsevier.com/locate/gloplacha

Research article

Aridification and orbital forcing of eastern African climate during the Plio-Pleistocene

C.J. Lepre [a,*], R.L. Quinn [a,b]

[a] Rutgers University, Department of Earth & Planetary Sciences, Piscataway, NJ 08854, USA
[b] Seton Hall University, Department of Sociology, Anthropology, Social Work and Criminal Justice, South Orange, NJ 07079, USA

ARTICLE INFO

Editor: Zhengtang Guo

ABSTRACT

We developed a composite outcrop proxy record of Plio-Pleistocene climate in eastern Africa using the radiometrically-dated sediments of the Omo Group that preserve evidence for early hominin evolution. New stable oxygen isotopic measurements from pedogenic carbonate nodules ($\delta^{18}O_{PC}$, $n = 270$) are added to the existing database for a total of 759 observations spanning a ~ 3.6 Myr interval from 4.33–0.65 Ma. Linear interpolation of sample positions between tuffaceous marker horizons produced the chronostratigraphy of the $\delta^{18}O_{PC}$ record that was correlated to Indo-Pacific marine core sediment records and astronomical solutions of orbital climate forcing. Rainfall/evaporation changes inferred from the $\delta^{18}O_{PC}$ record carry orbital eccentricity signals, and the amplitude modulation of short eccentricity (~100 kyr) predicted by the astronomical solutions is evident during some intervals. $\delta^{18}O_{PC}$ variations recover many of the ~100 kyr cycles between ~4.3–0.7 Ma, with chronostratigraphic offsets between the Omo Group time series and astronomical solutions usually within the resolution of the radiometric uncertainties, i.e., ≤ 50 kyr; however, missing time at ~1.2 Ma contributes to nearly 150 kyr of offset. These $\delta^{18}O_{PC}$ data also indicate a long-term drying trend beginning at 2.11 Ma that correlates to a thicker eastern Indian Ocean mixed layer and upwelling in the eastern Pacific, implying a simultaneous response across the tropics to strengthening Walker Circulation. Published $\delta^{13}C_{PC}$ values from the same pedogenic carbonate nodules indicate that C_4 vegetation abundances increased beginning at ~2.0 Ma, also suggesting climatic drying. Spectral analysis of the $\delta^{13}C_{PC}$ time series provides weaker evidence of orbital forcing as compared to the $\delta^{18}O_{PC}$ time series, particularly for long orbital eccentricity (405 kyr) and climatic precession (~20 kyr), suggesting other factors, such as feeding ecology of herbivores or global greenhouse gas, may have contributed to the vegetation patterns. The climatic precession component to the $\delta^{18}O_{PC}$ time series increases amplitude through strengthening Walker Circulation, which may signal a change in the intensity of interannual climate events. No indications were observed to suggest that the Plio-Pleistocene Northern Hemisphere glaciation resonated as either climatic cyclicity or an abrupt, stepwise shift in the regional hydroclimate. At major junctures of hominin evolution, including the origins of different genera and the earliest stone tools, environmental variability derived from the orbital forcing of the monsoon appears to have been low. However, we propose that at 2.11–1.66 Ma, directional aridity coupled with interannual climate events presented a new adaptive context where *Homo erectus* and Acheulian stone tools first appeared in eastern Africa.

1. Introduction

The evolution of hominins in eastern Africa is thought to have been closely connected with Plio-Pleistocene global climate change. Several different hypotheses have been put forth, and most studies typically implicate either Northern Hemisphere glaciation or the role of orbital insolation forcing as drivers of paleoenvironmental changes that impacted hominin habitats (Cane and Molnar, 2001; deMenocal, 2004; Maslin et al., 2014; Potts and Faith, 2015; Trauth et al., 2009). The onset of Pacific Walker Circulation and its effects on monsoonal precipitation also has been considered as an important cause of early hominin evolutionary events (Donges et al., 2011; Maslin and Trauth, 2009). However, there is considerable wavering about how Walker Circulation affects eastern African paleoclimate, with some hypotheses suggesting stronger Walker Circulation contributed to a period of mega-monsoons and large lakes at about 1.8 Ma, whereas others indicating increased

* Present address of the corresponding author at: School of Earth, Environment & Society, Bowling Green State University, Bowling Green, OH 43403
E-mail address: clepre@eps.rutgers.edu (C.J. Lepre).

https://doi.org/10.1016/j.gloplacha.2021.103684
Received 21 May 2021; Received in revised form 19 September 2021; Accepted 21 October 2021
Available online 26 October 2021

aridity caused by stronger Walker Circulation (Maslin et al., 2014; Trauth et al., 2021). In all these hypotheses, there has been limited discussion of the physical climatological processes that addresses how strengthening Walker Circulation impacted the Plio-Pleistocene African monsoon.

Another important constraint on the evolution of Plio-Pleistocene African climate was Indo-Pacific ocean temperatures and currents, as influenced by the tectono-paleogeography of the Maritime Continent (Cane and Molnar, 2001). Today, there is considerable interest in the Indo-Pacific area because of the influence that local ocean-atmospheric systems have on Earth's global climate (DiNezio et al., 2018; King et al., 2021; White and Ravelo, 2020) and the impact that Walker Circulation and its disruption by the El Niño Southern Oscillation and Indian Ocean Dipole events has had on historical changes to the interannual rainfall variability of the African monsoon (Molnar and Cane, 2002; Tierney et al., 2015; Yang et al., 2015). However, understanding current climatological trends has been challenging (Nicholson, 2017), and studies attempt to reconcile recent drought severity with model predictions of Walker Circulation and East African rainfall (King et al., 2021; Tierney et al., 2015). Therefore, more study is necessary to provide geologic data input on monsoonal conditions during known times of Walker Circulation change (Mohtadi et al., 2017).

The East African Rift System is known for many geological records of terrestrial ecosystem evolution and has accumulated sediment sequences with volcanic ash layers that can be radiometrically dated to provide detailed Plio-Pleistocene records of environmental change. Within the Turkana Basin of Kenya, for example, the chronostratigraphic age constraints allow for the recognition of orbital cyclicity from geochemical proxy indicators (Joordens et al., 2011; Lupien et al., 2020; Yost et al., 2021) and lithofacies cycles (Boës et al., 2019; Lepre et al., 2007; Nutz et al., 2017). Passey et al. (2010) was one of the first to suggest that the age constraints on the Turkana Basin sequences may help to resolve short eccentricity (~100 kyr) cycles from the stable isotopic composition of pedogenic carbonates. The chronostratigraphy also facilitates the correlation of marine geological records to terrestrial Kenya (Brown, 1995; Feakins et al., 2005; Lepre, 2014; Polissar et al., 2019; Uno et al., 2016). Therefore, the sediments of eastern Africa are valuable archives for studying monsoonal climate change (Deocampo et al., 2017; Renaut and Ashley, 2002), the context of human origins (Antón et al., 2014; Campisano et al., 2017), and how global and regional climate events impacted both (Cohen et al., 2016; deMenocal, 2004; Levin, 2015; Maslin et al., 2014; Potts and Faith, 2015; Trauth et al., 2009). However, a current observation that has been emerging is the possibility that Plio-Pleistocene environmental changes may have occurred in the absence of what was once thought to be increasing climatic aridity (Blumenthal et al., 2017; Passey et al., 2010; Polissar et al., 2019). There also has been considerable interest in understanding other controls on eastern African paleoecosystem change, such as discerning the contribution of climate and atmospheric pCO_2 concentration to paleoenvironmental patterns. The decrease in pCO_2 since the Miocene has been proposed as the primary cause for the rise and expansion of C_4 grasslands in Africa and change in ungulate grazer speciosity (Faith et al., 2018; Polissar et al., 2019).

To examine African paleoclimate and possible connections to human origins, we studied the Kanapoi, Nachukui, and Koobi Fora sedimentary formations in the Turkana Basin, Kenya and the correlative Shungura Formation in adjacent Ethiopia (Fig. 1). These formations span nearly 3.6 Myr, from 4.33 to 0.65 Ma (Fig. 2), and they overlap with the Mid-Pliocene Warm Period, the intensification of Northern Hemisphere glaciation, strengthening Walker Circulation, and the Mid-Pleistocene Transition (Fedorov et al., 2013). Our research provides a new stable oxygen isotope ($\delta^{18}O$) record of pedogenic carbonates (subscript PC) to study orbital climate forcing of the monsoon, compare with proxy records of Plio-Pleistocene conditions of the Indo-Pacific area, and

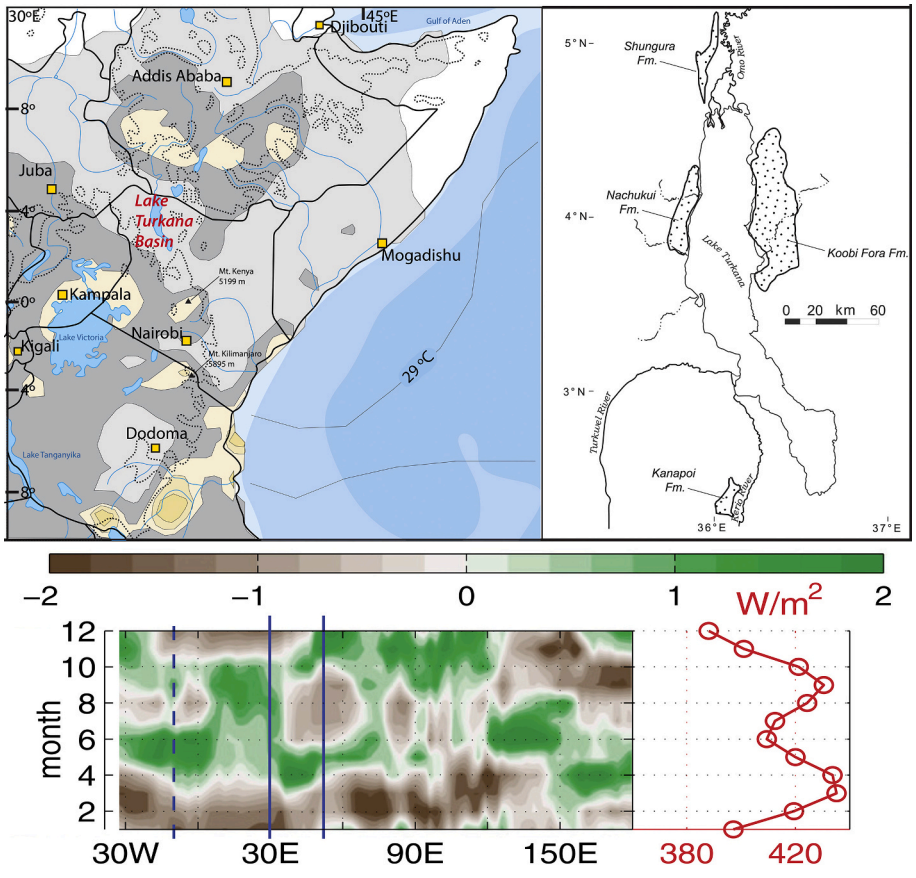

Fig. 1. Modern climate context and location of the studied Plio-Pleistocene sedimentary formations of the Omo Group. Left map showing precipitation and sea surface temperature (Yang et al., 2015). Darkening colors symbolize increasing rainfall: white to dark gray indicates 1 to 3 mm/day, light to dark tan indicates 5 to 9 mm/day. Data are for the "long" rains of March, April, and May. Thick lines are geopolitical boundaries. Boundary of NW Kenya adjacent to Sudan and Ethiopia is disputed. Dotted lines are elevations greater than about 1000 m. Right map indicates aerial distribution of principle outcrops of the Omo Group formations (Feibel et al., 1989; McDougall et al., 2012). Lower panel (Yang et al., 2015) shows top of the atmosphere insolation (W/m^2) paired to the monthly and seasonal rainfall at a single transect of 5 ° N latitude across the tropics (30 ° W to 150 ° E longitude). Vertical solid blue lines constrain 30–52 ° E. Vertical dashed blue line is where West Africa meets the coast. (For interpretation of the references to colour in this figure legend, the reader is referred to the web version of this article.)

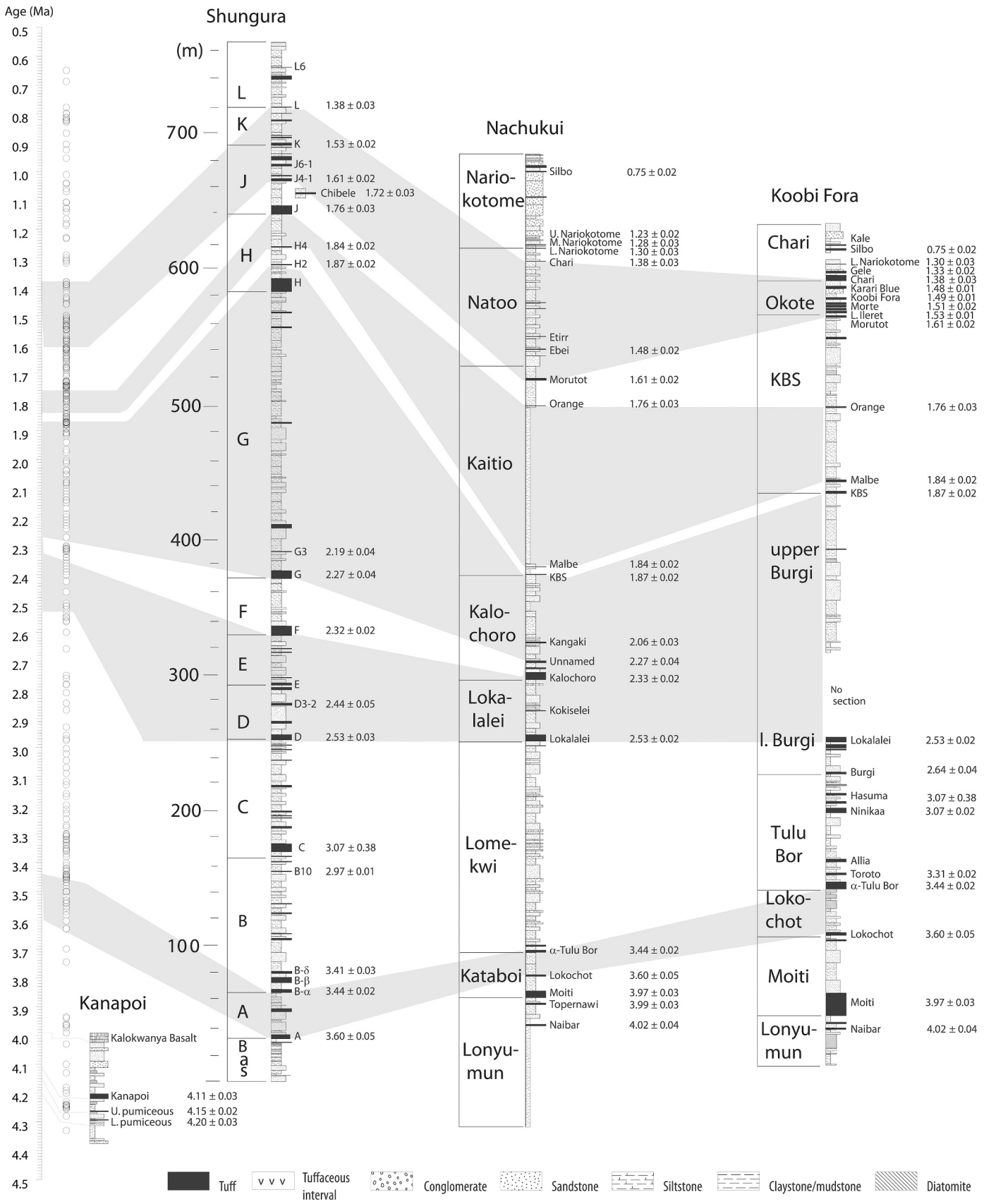

Fig. 2. Stratigraphic context of the $\delta^{18}O_{PC}$ samples (open circles next to age scale) used in this study, with emphasis on geochronology and correlation of tuffaceous marker horizons in the Omo Group formations (McDougall et al., 2012). Alternating shaded/white areas are defined by well-dated horizons that transcend the three formations. Tuffs F and G in the Shungura have correlatives in the Nachukui, but there is an unconformity within the Koobi Fora Formation that represents about 500 kyr of low/sediment accumulation. A similar unconformity occurs within the upper part of the Chari Member of the Koobi Fora Formation (Feibel et al., 1989).

interpret the causes of paleoenvironmental change in eastern Africa.

2. Materials and methods

2.1. Study area and pedogenic carbonate nodule samples

Northwest Kenya and southwest Ethiopia lies within a semi-arid environment that is between humid highlands of the East African Rift System (Fig. 1). This area of eastern Africa experiences two rainy seasons each year that, by and large, coincide with the vernal and autumnal equinoxes (King et al., 2021; Nicholson, 2018). Heavy rains fall during March-April-May, and milder ones occur in October-November-December (lower panel in Fig. 1). Rainfall derives from deep tropical convection and the landward inflow of moist monsoonal air from the western Indian Ocean, generated by seasonal insolation changes that contribute to the sensible heating of the continent (Nicholson, 2017) (Yang et al., 2015).

The studied Plio-Pleistocene sedimentary formations are part of the Omo Group (Fig. 1), which archive paleoenvironments that are analogous to modern Lake Turkana, the Omo Delta, and the Omo River (Brown and Feibel, 1991). A comprehensive stratigraphy and geochronology for the examined formations is well documented by previous research (Feibel et al., 1989; McDougall et al., 2012). These studies date the sediments to the Plio-Pleistocene, spanning the interval of 4.33–0.65 Ma (Fig. 2). Most radiometric ages for the formations are based on single-crystal dating of sanidine through the argon-isotope method, with reported dates having uncertainties at 50–10 kyr (McDougall et al., 2012). These sanidine crystals were mostly derived from volcanic pumice clasts (McDougall, 1985).

We compiled from the published literature (Cerling et al., 1988; Harmand et al., 2015; Levin, 2015; Levin et al., 2011; Patterson et al., 2019; Quinn et al., 2007, 2013; Quinn and Lepre, 2019, 2021; Wynn, 2000, 2004) the chronostratigraphic positions of 489 pedogenic carbonate nodules collected from the Omo Group and added these published $\delta^{18}O_{PC}$ values to our new $\delta^{18}O_{PC}$ dataset generated from 270 nodules. Previously published $\delta^{18}O_{PC}$ values used in this study were analyzed from paleosols in the Kanapoi, Nachukui, Koobi Fora, and Shungura formations; we contribute new $\delta^{18}O_{PC}$ values from the Nachukui and Koobi Fora formations (Fig. 2 **and Table S1**). Paleosols in these formations, many of which are paleo-Vertisols, have been previously identified (Lepre, 2017, 2019; Quinn et al., 2007, 2013; Quinn and Lepre, 2019, 2021) through the recognition of structures and horizons such as gilgai, vertic horizons, and slickensided peds (Lepre, 2017, 2019; Quinn et al., 2007, 2013; Quinn and Lepre, 2019, 2021). Sample levels were placed within the stratigraphic framework of the Omo Group by measuring the stratal thickness between a sample level and the base of the tuffaceous marker horizons portrayed in Fig. 2. We used a Jacob's staff and Brunton compass to measure the stratigraphic thickness of the exposed outcrops. To extract pedogenic carbonate nodules, we first identified the uppermost surface horizon of the paleosol and a position $\geq$30 cm below this surface horizon level from a distinct Bk. Then we excavated a small trench into this position that went $\geq$50 cm deep beyond the visually weathered zone. The nodules were then plucked from the trench walls with a fine digging tool and examined for size, shape, and integrity before sealed within fabric or plastic bags.

To assign ages to each $\delta^{18}O_{PC}$ value, we interpolated the chronostratigraphic position of the pedogenic carbonate nodule. We used linearly interpolated sediment accumulation rates to estimate the timing of the stratigraphic intervals between dated tuffaceous marker beds in Fig. 2. These calculations resolve uncompacted sediment accumulation rates and do not consider the dry bulk density of the sediments. Similar approaches have been employed by other researchers to infer ages of isotope samples or body fossils from the sedimentary formations we investigated (Feibel et al., 1989; Levin et al., 2011; Quinn et al., 2007, 2013; Wynn, 2004). See McDougall et al.(McDougall et al., 2012) and Feibel et al. (Feibel et al., 1989) for a detailed explanation of this linear interpolation approach for the Omo Group, which is referred to as stratigraphic scaling by these authors.

2.2. $\delta^{18}O_{PC}$ analysis and sources of variation

Pedogenic nodules were cross-sectioned to expose the inner surface. Carbonate powders were eroded with a hand-held rotary tool (Foredom Series) affixed with a 0.5 mm carbide bit. We avoided sparry calcite and collected micrite from the nodules. Paired $\delta^{13}C$ and $\delta^{18}O$ analyses of extracted powders from pedogenic carbonate nodules were conducted on a FISIONS Mass Spectrometer in the Department of Earth and Planetary Sciences at Rutgers University. Samples were reacted at 90 °C in 100% phosphoric acid for 13 min. $\delta^{13}C_{PC}$ values were previously published (Quinn et al., 2007, 2013). $\delta^{18}O_{PC}$ values are reported in the standard per mil (‰) notation: = (Rsample / Rstandard – 1) * 1000, relative to Vienna-Pee Dee Belemnite (V-PDB) using the laboratory standard NBS-19. Analytical error is <0.05‰.

Monsoonal seasonality causes soil temperature and moisture variations that influence $\delta^{18}O_{PC}$ values of nodules formed within horizons deeper than about 30 cm from the land surface (Cerling, 1984; Passey et al., 2010). $\delta^{18}O_{PC}$ values reflect rainfall source $\delta^{18}O$ values, rainfall amounts relative to evaporative loss, and soil temperatures during carbonate nodule formation (reviewed in Levin, 2015; Quade and Levin, 2013); however, these methods are limited to characterizing carbonate-bearing paleosols, which form with negative water budgets (Cerling, 1984; Birkeland, 1984; Quade et al., 1989). $\delta^{18}O_{PC}$ values are controlled by soil pore water $\delta^{18}O$ values and temperature-dependent isotopic fractionation (+0.22‰ per °C decrease) during carbonate formation (Cerling, 1984; Kim and O'Neil, 1997). At depths greater than 30 cm, soil pore water $\delta^{18}O$ values approximate those of meteoric water (Amundson and Wang, 1996; Cerling and Quade, 1993). Soil pore water $\delta^{18}O$ values can change from expected meteoric water $\delta^{18}O$ values due to evaporation (Cerling and Quade, 1993; Hsieh et al., 1998). Paleosols preserved in the Plio-Pleistocene Turkana Basin are dominated by Vertisols, formed under a dry season of four or more months and 250–1000 mm of annual moisture (Wynn, 2000). Vertisols of eastern Africa (Deckers et al., 2001) have high clay contents and shrink/swell in response to annual moisture changes, resulting in the characteristic deep, vertical cracks and angular, wedge-shaped peds with slickensides. Pedogenic nodules typically average environmental condition of 10^1–10^3 of years (Srivastava, 2001) and represent ~1 m of spatial extent (Monger et al., 2009). Pedogenic nodules primarily form in the warm season and differentially record times of soil dewatering (Breecker et al., 2009). Using the clumped isotope paleothermometer in the Turkana Basin, (Passey et al., 2010) found no directional shift in soil temperatures from 4 to 1 Ma. We interpret significant variations in the $\delta^{18}O_{PC}$ record were primarily controlled by evaporation relative to rainfall.

2.3. Time series analysis

The data curves portrayed in Fig. 3B are representative of our compiled $\delta^{18}O_{PC}$ dataset that comprises 759 observations spanning 4.33 to 0.65 Ma (**Table S1**). To identify significant shifts in this time series, Bayesian change point analysis (Ruggieri, 2013) was performed on a MATLAB platform using the software *Acycle* v2.2 (Li et al., 2019). We first used the "Sort/Unique/Delete-empty" function so that two or more data points with the same interpolated age were replaced by one mean $\delta^{18}O_{PC}$ value for that interpolated age. To calculate the posterior probability of a change point for the sorted $\delta^{18}O_{PC}$ dataset, we used *Acycle* default settings for 500 sampled solutions and a maximum of 10 change points allowed. See **Table S2** for the complete set of posterior probabilities and regression values.

To assess the presence of orbital climate cycles within the $\delta^{18}O_{PC}$ time series, power spectra analysis was performed with *Acycle* using the 2π multi-taper method (MTM) (Thomson, 1982). We first converted the 759 interpolated ages of the $\delta^{18}O_{PC}$ dataset (**Table S1**) from Ma to Ka (e.

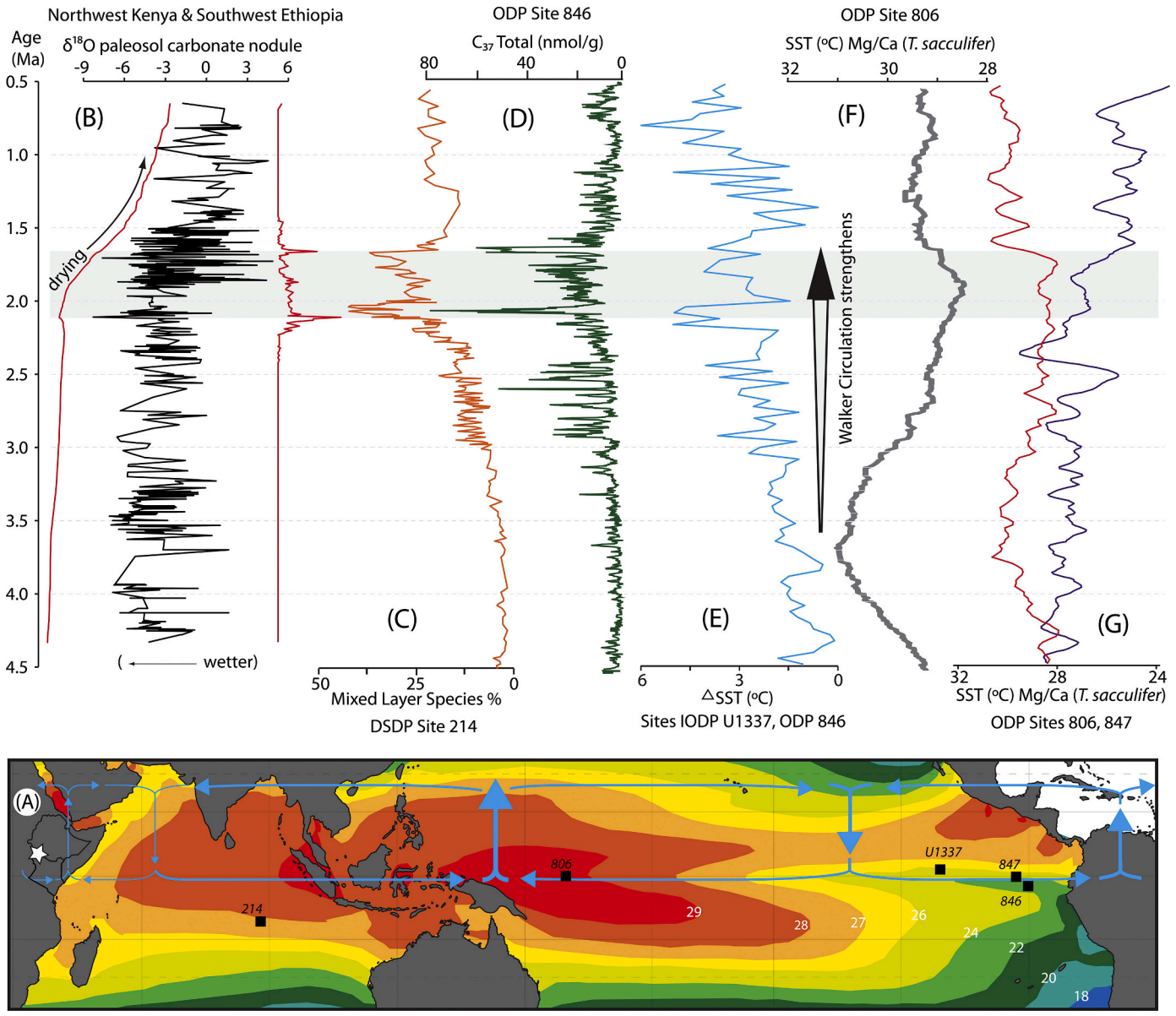

Fig. 3. Development of monsoonal climate change in eastern Africa through the onset of Walker Circulation. (**A**) Location of the Plio-Pleistocene paleosols and hominin sites (white star) in eastern Africa in relation to the Indo-Pacific marine sediment cores. ODP sites 806 and 847 are at the equator. Latitude increments are 10°; longitudes are 30°; dashed latitudes are the tropics. White numbers and ocean colour contours are annual mean SST for years 1971–2000. Blue arrows/lines represent the Walker Circulation patterns over the course of a "typical" year; both retrieved from NOAA.gov. (**B**) Plio-Pleistocene $\delta^{18}O_{PC}$ data time series (black line) compared with Bayesian change points (red line at right, maximum value of 0.098 posterior probabilities at 2.11 Ma) and regression model (red line at left) indicating drying trend. (**C**) Mixed layer species percentages (MLS%) from DSDP site 214 (Bali et al., 2020). (**D**) Organic productivity record (C_{37}) for the eastern equatorial Pacific (ODP site 846)(Lawrence et al., 2006). (**E**) Eastern Pacific Ocean cold tongue evolution appreciated by the SST gradient of sites IODP U1337 and ODP 846(Liu et al., 2019). (**F**) Corrected and recalibrated SST for ODP site 806(White and Ravelo, 2020). (**G**) Equatorial Pacific SST gradient for reference (Wara et al., 2005). (For interpretation of the references to colour in this figure legend, the reader is referred to the web version of this article.)

g., 4.33 Ma to 4330 Ka, 0.65 Ma to 650 Ka). We then used *Acycle* to sort, re-sample to 10 kyr increments, and de-trend the Ka $\delta^{18}O_{PC}$ time series. De-trending was done with a 25% LOWESS. This $\delta^{18}O_{PC}$ Ka time series was then subjected to the 2π MTM with three DPSS tapers, a zero-pad factor of five, and robust AR(1) red noise detection. Results of this are reported in Fig. 4A.

The same time series used for MTM was also examined with evolutive harmonics analysis (EHA) performed by *Astrochron* (Meyers, 2014). EHA settings were three 2π prolate tapers, a pad factor of 5000, 10 steps, and 800 window (right panel in Fig. 5).

Additionally, the Ka time series of 759 $\delta^{18}O_{PC}$ values was studied with a Blackman-Tukey coherency comparison (Fig. 4B) using *Analyseries* (Paillard et al., 1996). The target solution was daily summer insolation at 65° N (Laskar et al., 2004). *Analyseries* automatically sorts the data, and the Blackman-Tukey function linearly interpolates and re-samples the $\delta^{18}O_{PC}$ Ka time series on the basis of the insolation solution. For the analysis, we used a Bartlett-type window and a zero-base correlation coefficient of 0.5 (i.e., 80% significance level).

Spectral analysis of the La04 astronomical solutions (Laskar et al., 2004; Li et al., 2019) indicates that the main orbital periods of the late Cenozoic include 405 kyr (long eccentricity), 125 and 95 kyr (short eccentricity), 40.9 kyr (obliquity), and 22.4, 23.7, and 19.2 kyr (climatic precession). Precession and obliquity can be interpreted despite that the reported uncertainties for the Omo Group's radiometric dates are 10–50 kyr. Meaning that, although some of the radiometrically dated tuffs have uncertainties greater than precession and obliquity periods, other tuffs

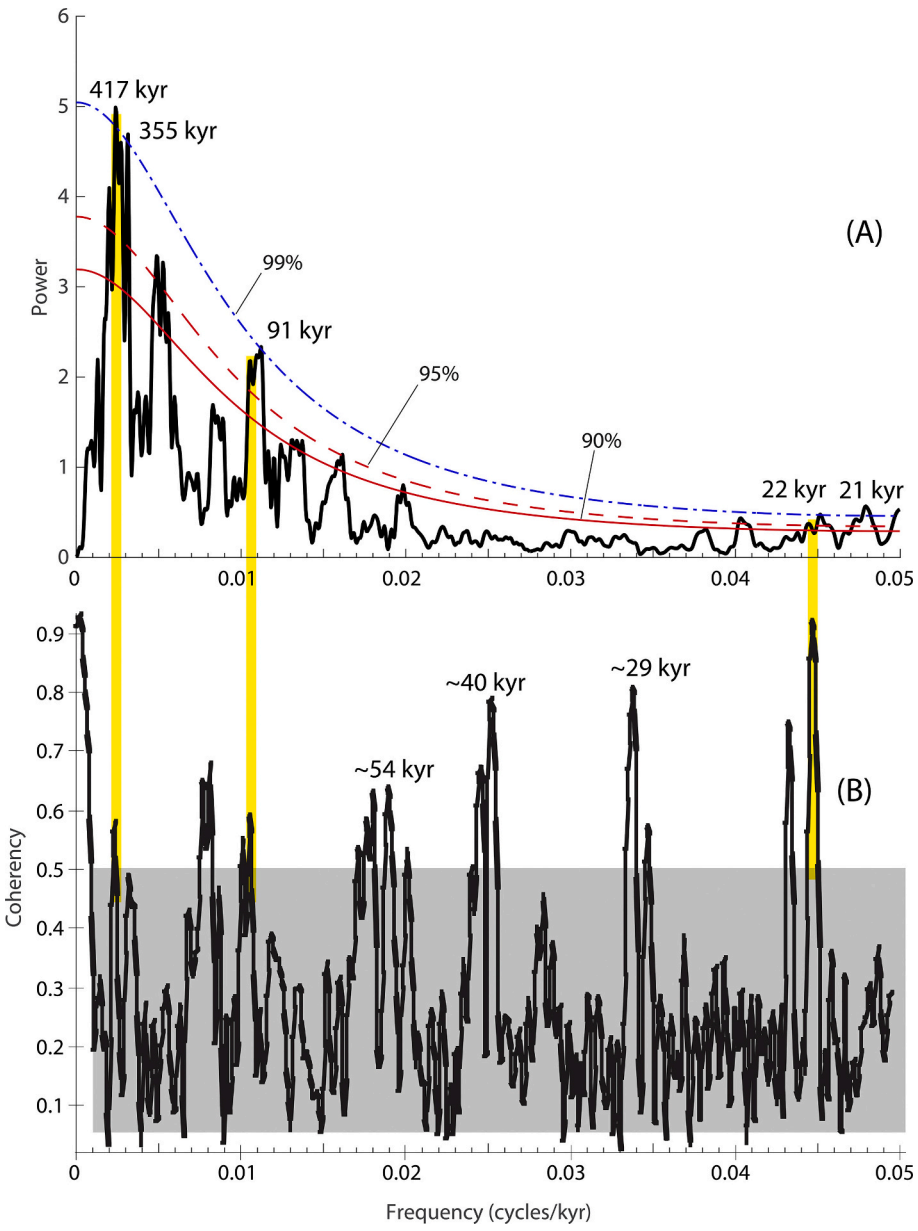

Fig. 4. Spectral analysis of the $\delta^{18}O_{PC}$ record. (**A**) Results of the 2π multi-taper method using the sorted and resampled $\delta^{18}O_{PC}$ time series treated to a 25% LOWESS. The labeled cycles in kyr are those that attain over 99% of significance. (**B**) Blackman-Tukey cross coherency (non-zero coherency at 0.5/80% indicated by gray box) between the $\delta^{18}O_{PC}$ time series and daily summer insolation at 65° N. Yellow vertical bars denote the orbital periods interpreted to be most significant, as defined by high confidence levels for both MTM and cross coherency results. Obliquity and its harmonic periods (Zeeden et al., 2019) are labeled on the Blackman-Tukey figure to emphasis their absence from the MTM results. (For interpretation of the references to colour in this figure legend, the reader is referred to the web version of this article.)

have smaller age uncertainties. Orbital cycles are frequently resolved from geological formations that lack any numerical age control, with effective uncertainties that are thus much less precise than the duration of the orbital periods. Precision of the uncertainties is an important consideration for calculating the absolute age difference between two vertically adjacent stratigraphic datums. The Omo Group's radiometric dates may help to discern the relative durations of orbital cycles with ~20–405 kyr periods but struggle to resolve empirically indistinguishable numerical ages for the stratigraphic datums that are <50 kyr apart.

Based on theory used for the spectral analysis of paleoclimatic stratigraphy, the shortest cycle detectable for a given time series is the Nyquist frequency (Kodama and Hinnov, 2015; Meyers, 2014). The Nyquist frequency is determined by the stratigraphic sample spacing. The equation for calculating the duration of the shortest cycle detectable is: Nyquist frequency = 1 / (2 × sample spacing). We expect to identify frequencies corresponding to climatic precession, which has late Cenozoic periods of 23.7, 22.4, and 19.2 kyr (Laskar et al., 2004; Li et al., 2019). The most precise uncertainty for the radiometric dates of the Omo Group is 10 kyr (McDougall et al., 2012), suggesting that the chronostratigraphic scheme we adopted may have the resolution for discerning cycle periods ≥20 kyr. The Nyquist frequency for the most precise uncertainty (0.05) is greater than Nyquist frequency for climatic precession (0.026–0.021). Our MTM results (Fig. 4A) indicate two significant periods at 22 and 21 kyr that achieve the 99% confidence level. These periods correlate to late Cenozoic climatic precession averages (Laskar et al., 2004; Li et al., 2019) of 21.8 kyr (average of 23.7, 22.4, and 19.2 kyr) and 20.8 kyr (average of 22.4 and 19.2 kyr).

2.4. $\delta^{18}O_{PC}$ comparisons to marine sedimentary records

We compared the $\delta^{18}O_{PC}$ time series with marine sedimentary records that span the Plio-Pleistocene (Fig. 3). Chronostratigraphic observations were used to assess correlations between the timing of changes in $\delta^{18}O_{PC}$ values and tropical paleoclimate. The three marine sites selected (Fig. 3A, C-3G) were the eastern Indian Ocean (DSDP 214), the western Pacific (ODP 846), and the eastern Pacific Ocean (IODP U1337, ODP 846 and 847). Sediment cores from the eastern and western Pacific provide information on tropical sea surface temperature and

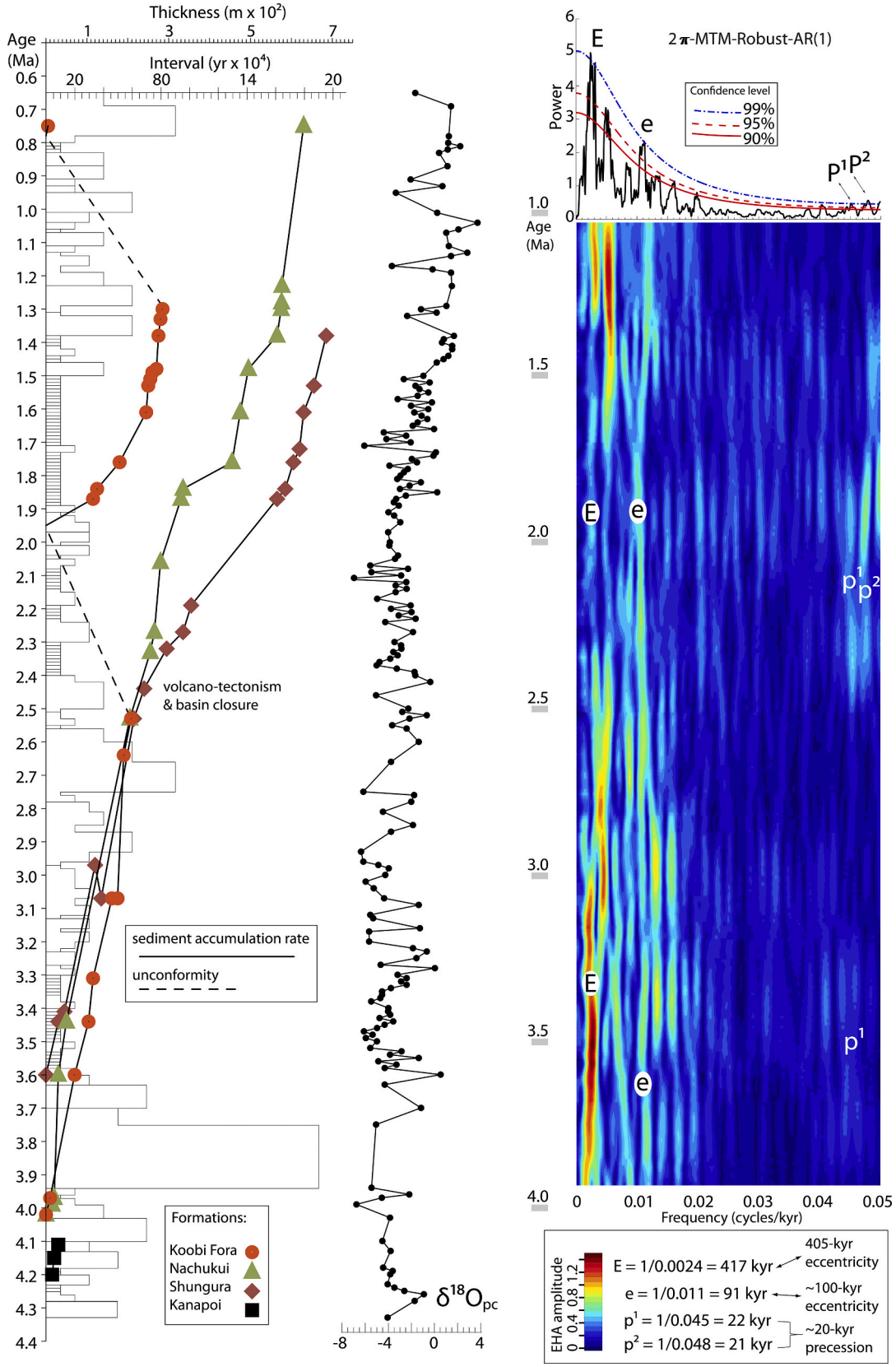

Fig. 5. Evolutive harmonics analysis of the Plio-Pleistocene Omo Group $\delta^{18}O_{PC}$ record. Left—Stratigraphic age control and sample density of pedogenic carbonate nodules from the Kanapoi, Nachukui, Shungura, and Koobi Fora sedimentary formations. Colored geometric symbols are radiometric dates (Fig. 2) plotted against stratal thickness (i.e., sediment accumulation rate). Note basin impoundment and sedimentation change near 2.5 Ma [see discussion in (Lepre, 2014)]. Bar height and length denote stratigraphic sampling interval in time (e.g., large gap centered at ~3.85 Ma is 18 × 10^4 years). Middle—the sorted $\delta^{18}O_{PC}$ time series. Top Right—2π MTM result as in Fig. 4A. Right—Evolutive harmonics analysis (step: 10 kyr, window: 800 kyr) of the $\delta^{18}O_{PC}$ time series.

marine upwelling. The eastern Indian Ocean core has been used to reconstruct the Plio-Pleistocene evolution of the mixed layer. Paleoclimate and paleoceanographic records from these tropical sites are used to infer the behavior of Walker Circulation patterns across the equatorial tropics (Fig. 3A).

3. Results and interpretations

3.1. Long-term trends of $\delta^{18}O_{PC}$

We observe no correlation between the sediment accumulation rate changes and the $\delta^{18}O_{PC}$ record (left panel in Fig. 5). There is no shift of isotopic values aligning with increased/decreased sedimentation accumulation rates. Besides the unconformities within the Koobi Fora Formation, the largest change in sediment accumulation rates occurs at ~2.5 Ma, particularly within the Shungura Formation, and there are comparatively minor sediment accumulation rate changes at ~1.8 Ma and ~ 1.5 Ma in the Nachukui Formation. Between 2.5 and 1.4 Ma, the Shungura Formation accumulates over 400 m of sediment. Prior to this, at 3.6–2.4 Ma, the Shungura accumulates about 300 m of sediment. This indicates an increase of the sediment accumulation rate by a factor of 1.6, from 25 cm/kyr in the Late Pliocene to 40 cm/kyr into the Early Pleistocene. In the $\delta^{18}O_{PC}$ record the change with the greatest significance occurs at 2.11 Ma (Fig. 3B**; Table S2**). Therefore, based on the largest change in sedimentation rate predating the change in the $\delta^{18}O_{PC}$ record, we interpret that these shifts are unrelated geologically and paleoenvironmentally.

Our $\delta^{18}O_{PC}$ time series of the Omo Group comprises 759 observations spanning 4.33 to 0.65 Ma (**Table S1**). The $\delta^{18}O_{PC}$ values average to −2.4‰ and range from −8.3 to 4.9‰ over the ~3.6 Myr period of the record (Table 1). Posterior probabilities indicate that the likeliest change points of the $\delta^{18}O_{PC}$ record occur at 2.11 and 1.66 Ma (**Table S2**), with the Bayesian regression curve showing increasing $\delta^{18}O_{PC}$ values beginning near 2.11 Ma (Fig. 3B). These isotopic patterns suggest a shift towards a drier paleoclimate that appears to have coincided with significant strengthening of Walker Circulation in the Pacific and probably Indian oceans (Figs. 3B-G).

Isotopic change at 2.11–1.66 Ma is followed by a continued but more gradual increase in $\delta^{18}O_{PC}$ values that suggest the driest conditions of the entire record developed at 1.65–0.65 Ma (Fig. 3B**)**. The Turkana $\delta^{18}O_{PC}$ record shows a short-term excursion towards lower values during the Mid-Pleistocene Transition (Quinn and Lepre, 2021), but overall the 1.65–0.65 Ma part of the record has some of the highest $\delta^{18}O_{PC}$ values with an average of −0.6‰ (Table 1). In contrast, the Early Pliocene (4.3–3.2 Ma) is interpreted as experiencing wet conditions that are characterized from a $\delta^{18}O_{PC}$ average of −3.9‰ (Table 1). Less negative $\delta^{18}O_{PC}$ values are prominent during this wet interval at 4.13, 3.70, 3.60, 3.53, and 3.23 Ma (Fig. 3B), suggesting episodic drying. Within the Mid-Pliocene Warm Period at 3.2–2.8 Ma, there is a modest change to more negative $\delta^{18}O_{PC}$ values (average $\delta^{18}O_{PC}$ = −4.7‰) that may suggest overall wetter conditions, although the sample size is relatively small (Table 1).

Through the intensification of Northern Hemisphere Glaciation at 2.8–2.2 Ma, the $\delta^{18}O_{PC}$ values increase to a mean of −3.1‰, which suggests drier conditions as compared to the Mid-Pliocene Warm Period at 3.2–2.8 Ma (Table 1). Distinctive dry peaks are centered at 2.78, 2.56, 2.40, 2.32, 2.23, 2.12 Ma (Fig. 3B). The drying conditions through the interval of 2.8–2.2 Ma appear to be part of larger yet gradual trend towards higher $\delta^{18}O_{PC}$ values that began near ~3.5 Ma, according to the Bayesian regression curve associated with the results of change point analysis (Fig. 3B**, Table S2**). Some studies observe gradual nutricline and thermocline shoaling and cooling of the eastern equatorial Pacific at this time (Ford et al., 2015; Jakob et al., 2021; Wara et al., 2005) but a possible impact on African climate has not be discussed. However, there is no indication of a shift in the $\delta^{18}O_{PC}$ record that suggests Northern Hemisphere Glaciation led to an abrupt, stepwise increase of African aridity, like some marine core aeolian records demonstrate (deMenocal, 2004; Liddy et al., 2016). Moreover, it is uncertain where and if the aeolian detritus contained in the marine core records originated from the rift valley of eastern Africa. Radiogenic study of Holocene dust flux suggests that, rather than interior eastern Africa, coastal areas are the more likely sources for the aeolian detritus transported to the marine core sites (Jung et al., 2004). It has been assumed that the presence of the same volcanic ashes within the marine core records and the rift valley lake basins suggest that the windblown detritus of the cores derived from hominin sites of the rift (Feakins et al., 2005; Uno et al., 2016). However, volcanic paroxysms responsible for the dissemination of the ash are not analogous to the processes of aeolian transport from continental eastern Africa to the marine realm. We also do not see a change that suggests the climate humidified because the tropical rainfall belt was latitudinally shifted by the new pole-equator temperature gradient during the intensification of Northern Hemisphere glaciation (Caley et al., 2018; Maslin and Trauth, 2009). In the central rift valley of Kenya, study of the carbon isotopic composition of leaf wax biomarkers in the Chemeron Formation (~0.5° N) suggests a wetter Pliocene followed by a progressively drier climate culminating with an abrupt expansion of C_4 grasslands at ~3.04 Ma (Lupien et al., 2021) Two recent comprehensive analyses of large datasets based on floral and faunal stable isotopic records from the Turkana Basin (Quinn et al., 2021; Quinn and Lepre, 2021) showed a gradual drying trend across the Plio-Pleistocene boundary but failed to recognize a stepwise increase of aridity suggestive of an abrupt C_4 grassland expansion at ~3.0 Ma. Such differences between the paleoenvironmental records may be explained by the Chemeron depositional systems had a heightened sensitivity to regional/global climate change because of their smaller aerial extent and catchment (Feibel, 1999). The Chemeron depositional system and catchment was likely <10,000 km^2, whereas the Omo Group's floodplain and lake-margin paleosols represent an integrated rainfall signal from sedimentary deposits exposed across an area of some 20,000 km^2 of northwest Kenya and southwest Ethiopia.

Table 1
Descriptive statistics and interval averages.

Average $\delta^{18}O_{PC}$ value ±1σ (complete record, n = 759)	−2.4 ± 2.4‰
$\delta^{18}O_{PC}$ value range (complete record, n = 759)	−8.3 to 4.9‰
Early Pliocene (4.3–3.2 Ma, n = 171)	−3.9 ±
Average $\delta^{18}O_{PC}$ value ±1σ	1.7‰
Mid-Pliocene Warm Period (3.2–2.8 Ma, n = 19)	−4.7 ±
Average $\delta^{18}O_{PC}$ value ±1σ	1.5‰
Northern Hemisphere Glaciation (2.8–2.2 Ma, n = 77)	−3.1 ±
Average $\delta^{18}O_{PC}$ value ±1σ	1.6‰
Walker Circulation Strengthening (between $\delta^{18}O_{PC}$ record changepoints, 2.11–1.66 Ma, n = 387)	−2.1 ± 2.2‰
Average $\delta^{18}O_{PC}$ value ±1σ	
Middle Pleistocene (post changepoint until end of record, 1.65–0.65 Ma, n = 219)	−0.6 ± 2.0‰
Average $\delta^{18}O_{PC}$ value ±1σ	

3.2. Spectral analyses

The 2π MTM power spectra for the $\delta^{18}O_{PC}$ data suggest the presence of orbital climate cycles within the time series (Fig. 4A). Orbital eccentricity and climatic precession are interpreted from frequencies with 99% significance at 0.0024 cycles/kyr (417 kyr), 0.011 cycles/kyr (91 kyr), 0.045 cycles/kyr (22 kyr), and 0.048 cycles/kyr (21 kyr). The 2π MTM results reveal no indications of the main ~40 kyr period of obliquity for the late Cenozoic.

Coherency results from Blackman-Tukey analysis (Fig. 4B) show that frequencies approximating long orbital eccentricity (435 kyr), short orbital eccentricity (123–95 kyr), and climatic precession (23–22 kyr) are significant. However, obliquity at the ~40 kyr period and obliquity

harmonics at ~54 kyr and ~ 29 kyr (Zeeden et al., 2019) are indicated by the Blackman-Tukey results as significant. Results from MTM (Fig. 4A) do not indicate significant frequencies that correlate to these periods. We therefore interpret the evidence for obliquity in the $\delta^{18}O_{PC}$ time series as speculative because, unlike eccentricity and precession, its identification is not method independent. Weedon (Weedon, 2003) suggests that significant coherency at frequencies where no significant spectral peaks are present indicates similar behavior for the two time series variables but that the oscillations are due to continuum noise rather than regular cyclicity.

MTM and Blackman-Tukey methods largely produce the same periodicities that approximate long eccentricity (405 kyr), short eccentricity (~100 kyr), and climatic precession (~20 kyr). Prior studies of Early Pleistocene lacustrine sediments of the Turkana Basin focusing on lithofacies cycles (Boës et al., 2019; Lepre et al., 2007; Nutz et al., 2017), strontium isotopes (Joordens et al., 2011), and vegetation remains (Lupien et al., 2020; Yost et al., 2021) have demonstrated orbital climate forcing by eccentricity and precession. None of these prior studies report evidence for glacial cyclicity or obliquity. Orbital eccentricity and climatic precession are expected to be strong controls of insolation budgets that force monsoonal climate change of large tropical landmasses (Olsen et al., 2019). We infer that ~100 kyr short eccentricity cycle is an insolation signal because only a portion of the $\delta^{18}O_{PC}$ time series covers the Mid-Pleistocene Transition when the power of ~100 kyr glacial-interglacial cycles increases in many marine paleoclimate records.

According to the EHA model (Fig. 5), the interpreted cycle of long eccentricity (405 kyr) has high amplitude between ~4.0 and ~ 3.0 Ma, but weakens at ~3.0 Ma and remains so until after 1.5 Ma. Short eccentricity (~100 kyr) is the most consistent as compared to climatic precession and long eccentricity, as it generally has the same amplitude and frequency through the entire EHA model (Fig. 5). Precession undergoes an increase in amplitude between about 2.5 and 1.7 Ma, but is comparatively low through the EHA model (Fig. 5). There is a smaller increase of precession amplitude at ~3.6–3.3 Ma.

Changing EHA patterns of long eccentricity and precession amplitudes may reflect changing sedimentary conditions. They can also derive from climate feedbacks or the modulation effects of orbital processes. A shift to higher frequency cycles is expected with a condensed section or when the sedimentation rate slows (Meyers et al., 2001). However, this seems unlikely for the Omo Group data because the Shungura and Nachukui sedimentation rates either stay the same or increase through 2.5–1.7 Ma when precession increases amplitude (Fig. 5). The Koobi Fora Formation has an unconformity at ~2.5–2.0 Ma but the sedimentation rate at ~1.9–1.6 Ma is faster than before the unconformity. There are no major decreases in the sedimentation rate during the changing character of long eccentricity at ~3.0 Ma (Fig. 5). At ~3.6–3.3 Ma and again at ~2.5–1.5 Ma (Fig. 5) increased amplitudes for climatic precession may be related to a change in the recurrence rate and/or the intensity of the positive Indian Ocean Dipole mode. A progressively more positive mode is predicted to generate wetter monsoonal conditions and increase the precession signal at northeastern African sites adjacent to the western Indian Ocean (Caley et al., 2018; Johnson et al., 2016).

We obtained the La04 eccentricity solution (Laskar et al., 2004) from *Analyseries* in order to compare with the $\delta^{18}O_{PC}$ dataset. We correlate more positive $\delta^{18}O_{PC}$ values with eccentricity minima, and eccentricity maxima with less positive $\delta^{18}O_{PC}$ values. The "linage" function of *Astrochron* was used to help with the comparisons. A higher concentration of the ^{18}O isotope indicates less replenishment of the ^{16}O isotope and less rainfall relative to evaporation. Orbital climate theory and geologic data predict that eccentricity maxima are correlated to increased rainfall at low latitude sites in Africa (Hilgen, 1991; Rossignol-Strick et al., 1982). With a more eccentric orbit, the seasonality effects from climatic precession are enhanced, usually increasing the rainfall. Less eccentric orbits decrease the seasonal disparities. We thus match lower/higher $\delta^{18}O_{PC}$ values with maxima/minima in the La04 eccentricity solution (Fig. 6).

Eccentricity cycles are apparent in the non-astronomically-tuned $\delta^{18}O_{PC}$ time series. The $\delta^{18}O_{PC}$ time series recapitulates individual short eccentricity cycles and shows amplitude changes in accordance with long eccentricity cycles (Fig. 6). To illustrate these features, three example intervals of the $\delta^{18}O_{PC}$ time series are shown in detail (Figs. 7, 8 and 9). One of these intervals, at 2.8–3.7 Ma, records nine short eccentricity (~100 kyr) cycles apparent in the astronomical solution (Fig. 7). $\delta^{18}O_{PC}$ amplitudes are relatively decreased at long eccentricity (405 kyr) cycle minima and relatively increased when long eccentricity increases amplitude. Amplitude modulation is better defined by the $\delta^{18}O_{PC}$ data at ~3.3–3.7 Ma. The next example interval at ~1.5–2.3 Ma (Fig. 8) is characterized by comparatively lower amplitude oscillations in the $\delta^{18}O_{PC}$ record and a paucity of evidence to suggest amplitude modulation by the long (405 kyr) eccentricity cycle. A substantial change of $\delta^{18}O_{PC}$ values indicates increasing dryness at 2.11 Ma (Fig. 3B and **Table S1**). The changeover at 2.11 Ma begins with the most negative (least dry) value of −8.3‰ in the entire $\delta^{18}O_{PC}$ record, which is constrained by the Kangaki Tuff (2.06 ± 0.03 Ma) and Tuff G3 (2.19 ± 0.04 Ma) and correlated to an eccentricity maximum centered near 2.12 Ma (Fig. 8). Another large negative value (−6.2‰) dated to 1.71 Ma is constrained by the Morutot Tuff (1.61 ± 0.02 Ma) and the Orange Tuff (1.76 ± 0.03 Ma) and correlated to an eccentricity maximum centered at ~1.74 Ma (Fig. 8). Strengthening Walker Circulation near 2.0 Ma (Etourneau et al., 2010) co-occurs with extreme cooling events of tropical SST at 2.1 Ma and again near 1.7 Ma (Herbert et al., 2010). Therefore, the $\delta^{18}O_{PC}$ oscillations through the interval of ~1.5–2.3 Ma may represent increasing teleconnectivity with Indo-Pacific hydroclimate systems. Results of the EHA model for the $\delta^{18}O_{PC}$ record (Fig. 5) suggest a higher amplitude for precession at ~1.5–2.3 Ma, which possibly signals greater sensitivity of the eastern African monsoon to seasonal/interannual climate events of the Indian Ocean basin (Johnson et al., 2016) at the expense of orbital modulation from eccentricity.

A third example interval is at ~0.8–1.5 Ma (Fig. 9), when the astronomical solutions show seven short eccentricity cycles bundled into sets of two and three. This chronostratigraphic interval of the Omo Group is noted for having an unconformity within the Koobi Fora Formation that represents low/no sediment accumulation lasting about 500 kyr (Figs. 2 and 5). It has been assumed that other formations in the basin lack such a diastema (Brown and Feibel, 1991; Harris et al., 1988; McDougall et al., 2012). However, a large timing offset between the $\delta^{18}O_{PC}$ cycles and the astronomical solution occurs at ~0.8–1.5 Ma (Fig. 9) that may be explained by incomplete preservation of stratigraphic section and thus time missing from the Nariokotome Member of the Nachukui Formation. This member has limited chronostratigraphic control points, especially for the interval of 0.75–1.30 Ma, which is where the Koobi Fora Formation unconformity lies (**Figs. 2** and **5**). Most of the Omo Group's $\delta^{18}O_{PC}$ data that dates to 0.75–1.38 Ma derive from the Nariokotome Member (Quinn and Lepre, 2021). Furthermore, we also note that the astronomical solution at 1.1–1.3 Ma indicates a pair of short eccentricity cycles whereas we interpret that the corresponding interval of the $\delta^{18}O_{PC}$ time series exhibits only one (Fig. 9). This single $\delta^{18}O_{PC}$ cycle is interpreted as an amalgam of the two astronomical cycles; however, it is likely that one of the two $\delta^{18}O_{PC}$ cycles is completely missing, if not more of the Omo Group record.

4. Discussion and implications for hominin evolution

4.1. Strengthening of Plio-Pleistocene Walker Circulation

Major reorganization of the ocean-atmospheric systems of the tropical and subtropical regions occurred through the Late Pliocene and Early Pleistocene (Fedorov et al., 2013; Maslin et al., 2014). This included the strengthening of the zonal Walker Circulation (WC) that prevails over the Indian and Pacific oceans (Fig. 3A). With exceptions (Scroxton et al., 2011; Zhang et al., 2014), multiple studies have

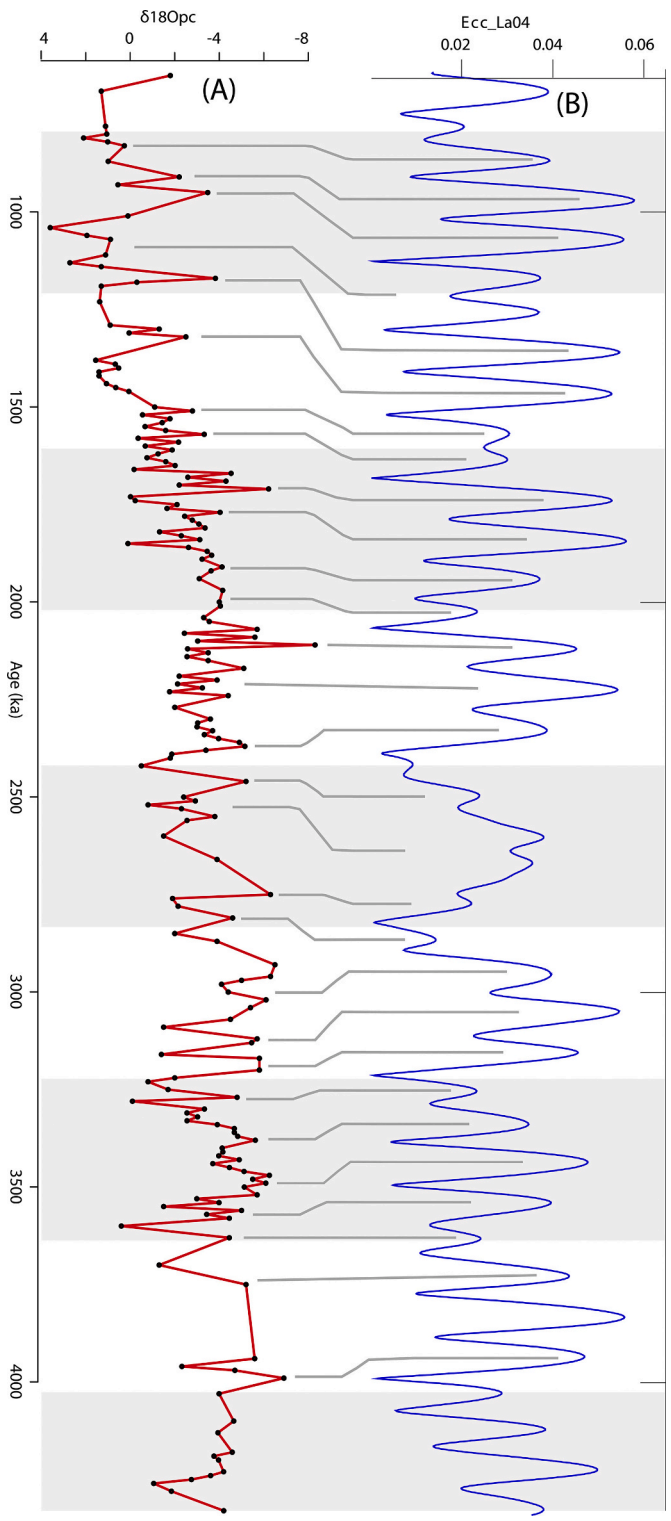

Fig. 6. Comparison of the $\delta^{18}O_{PC}$ time series to orbital eccentricity. (A) The sorted $\delta^{18}O_{PC}$ time series. Note that the isotope scale has been flipped from convention so that lower $\delta^{18}O_{PC}$ values (more rainfall) rise with eccentricity maxima. (B) Astronomical solution for eccentricity (Ecc_La04) at 4.33–0.65 Ma (Laskar et al., 2004). Alternating gray and white boxes denote approximate positions for the 405 kyr long eccentricity cycle. Gray lines are proposed correlations between peaks in the $\delta^{18}O_{PC}$ time series and short (~100 kyr) eccentricity maxima.

interpreted a weak WC during the Pliocene at 5–3 Ma, which is often said to be coeval with "permanent El Niño–like" conditions (Fedorov et al., 2013; Molnar and Cane, 2002; Tierney et al., 2019; Wara et al., 2005). Evidence suggests that change to the zonal sea surface temperature (SST) gradient experienced the largest increase between ~2.2 and 1.8 Ma ago, followed by the establishment of a WC intensity similar to the present-day emplaced by ~1.5 Ma (Etourneau et al., 2010; Ravelo, 2006; Wara et al., 2005). Other research demonstrates an earlier intensification coinciding with the development of large Northern Hemisphere ice sheets at ~3.0 Ma (Lawrence et al., 2006). Regional SST gradients associated with present-day WC appear to have formed at 3–2 Ma (Liu et al., 2019). Our $\delta^{18}O_{PC}$ data clearly suggests a shift towards less rainfall at 2.11 Ma, signaling the development of a drier monsoon for eastern Africa during strengthening WC (Fig. 3B-G).

Modern WC is typified by strong westerly surface winds along the equatorial Indian Ocean and easterlies over the equatorial Pacific Ocean (Lau and Yang, 2002). Wind vectors are generated by the SST asymmetries, characterized by the eastern equatorial Indian and western equatorial Pacific being warmer than the western Indian and eastern Pacific waters (Kang et al., 2020). The WC convection cells across the tropical Indian and Pacific oceans are initiated at the Maritime Continent, where warm and moist parcels of air rise and diverge within the troposphere towards the east and west (DiNezio and Tierney, 2013). Warm ocean water surrounding the Maritime Continent is referred to as the Indo-Pacific Warm Pool, and its area, temperature, and depth has effects on WC changes, as well as monsoon systems, the El Niño-Southern Oscillation, the mode of Indian Ocean Dipole, and the global climate system (Cai et al., 2013; Mohtadi et al., 2017; Molnar and Cane, 2002). Changing temperature of the Indo-Pacific Warm Pool and the associated zonal SST gradients across the Indian and Pacific oceans exert a strong control on the intensity of the WC along the equator (DiNezio and Tierney, 2013). WC strength increases (decreases) as the west-to-east SST gradient along the Indian Ocean increases (decreases) (Mohtadi et al., 2017). This gradient is sustained, in part, by the Indonesian Throughflow region that passes heat into the eastern Indian Ocean and less salty water and from the western Pacific north of the equator (Gordon and Fine, 1996). Assemblage of the Maritime Continent and related oceanographic features are purported to have established Indonesian seaway currents, changing the Indian Ocean SST gradient in concert with tectonic-geographic events (Molnar and Cane, 2002). These changes may have aridified the monsoon and affected human evolution in eastern Africa (Cane and Molnar, 2001).

Atmospheric circulation over the eastern Indian Ocean influences thermocline depth and mix layer thickness (Di Nezio et al., 2016). A thicker mixed layer is associated with stronger WC (Mohtadi et al., 2017). A thickening mixed layer of the eastern Indian Ocean was coeval with intensified WC at ~3.15–1.6 Ma (Bali et al., 2020). The strengthening WC appears to have peaked near 2 Ma, as significant increases happened at 2.2–2.0 Ma and again at 1.8–1.6 Ma (Bali et al., 2020). These events correlate in time almost precisely with our Bayesian change points in the $\delta^{18}O_{PC}$ time series (Figs. 3B, C).

At ~3 Ma, changes to mixed-layer taxa abundances in the eastern Indian Ocean are nearly synchronous with increasing primary production in the eastern Pacific Ocean (Figs. 3C, D). Eastern equatorial Pacific primary productivity also experiences two pronounced increases at ~2.1 and ~ 1.7 Ma (Herbert et al., 2010; Lawrence et al., 2006). At ~2.2 to 2.0 Ma, the western equatorial Pacific SST was stable yet the zonal Pacific SST gradient increased by 3–4 °C because of cooling in the eastern equatorial Pacific (Etourneau et al., 2010). This cooling in the eastern equatorial Pacific has implications for the primary productivity increases at ~2.1 and ~ 1.7 Ma (Fig. 3D) because cold up-welled water supplies surface nutrients. Cold up-welled water of the eastern equatorial Pacific has extra-tropical sources from the Southern Hemisphere. Model data and proxy records (Kang et al., 2020; Liu et al., 2019) suggest that WC strengthens from extra-tropical cooling of the eastern Pacific Ocean, which increases the SST gradient across the equatorial

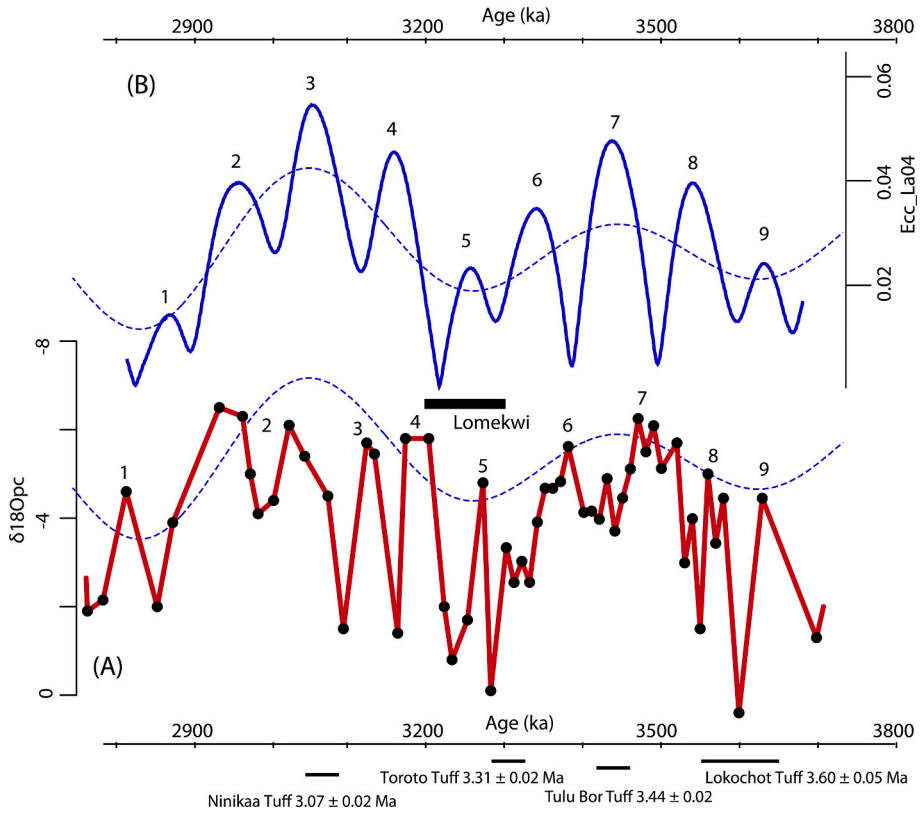

Fig. 7. Detailed comparison between astronomical solutions and the $\delta^{18}O_{PC}$ time series at 2.8–3.8 Ma. (A) sorted $\delta^{18}O_{PC}$ time series. Lomekwi and black bar represent chronostratigraphic position of the oldest known stone tools in the world yet discover (Harmand et al., 2015). Tuff dates and errors as in Fig. 2. (B) long and short eccentricity as in Fig. 6.

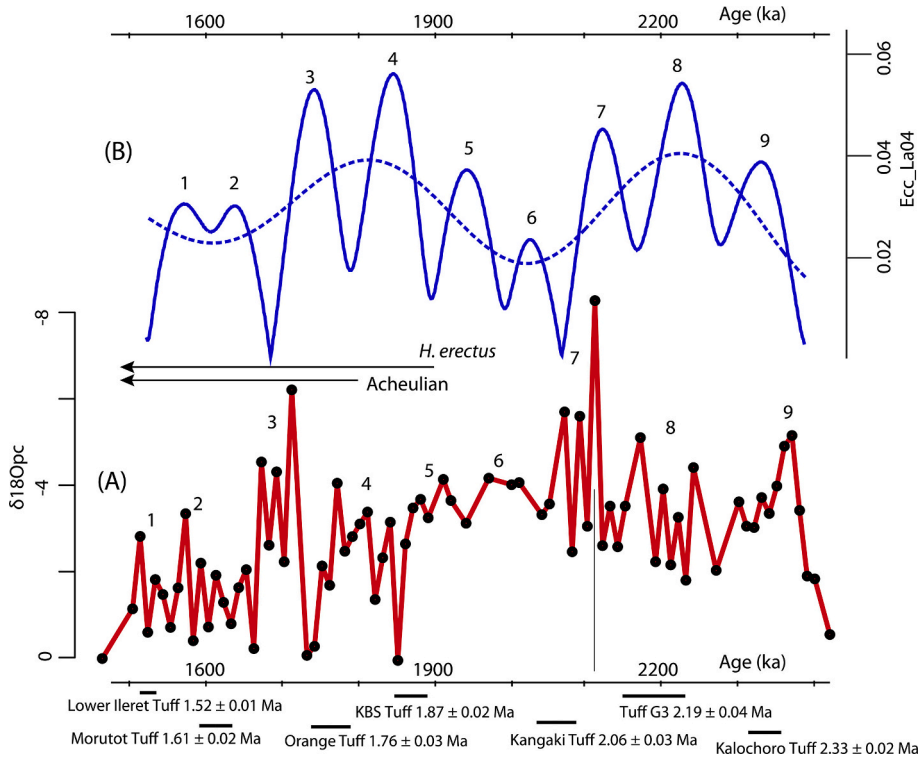

Fig. 8. Detailed comparison between astronomical solutions and the $\delta^{18}O_{PC}$ time series at 1.5–2.4 Ma. (A) sorted $\delta^{18}O_{PC}$ time series. Arrows indicate the first appearance of *H. erectus* and Acheulian stone tools in eastern Africa (Lepre et al., 2011; Lepre and Kent, 2015). Vertical gray lines denotes changepoint in the $\delta^{18}O_{PC}$ time series (Fig. 3B) that indicates the onset of climatic drying at 2.11 Ma. Tuff dates and errors as in Fig. 2. (B) long and short eccentricity as in Fig. 6.

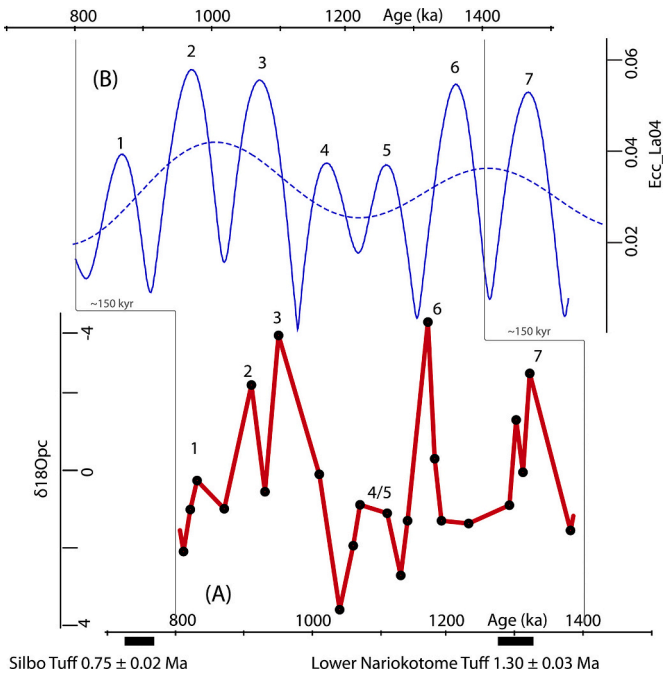

Fig. 9. Detailed comparison between astronomical solutions and the $\delta^{18}O_{PC}$ time series at 0.7–1.5 Ma. (A) sorted $\delta^{18}O_{PC}$ time series. Tuff dates and errors as in Fig. 2. (B) long and short eccentricity as in Fig. 6. Vertical gray lines denote the interpreted time offset by about 150 kyr between the two records. The two ~100 kyr eccentricity cycles at 1.1–1.3 Ma are shown as amalgamated in $\delta^{18}O_{PC}$ time series, but it is likely that one of the two cycles (if not more time) is completely missing from our isotopic record. The diastema may be related to the documented Omo Group unconformity representing low/no sediment accumulation at ~0.8–1.3 Ma (Figs. 2 and 5).

Pacific. These data collectively propose that extra-tropical cooling causes WC to intensify, evoking a simultaneous climate change in western South America, across the equatorial tropics, and into eastern Africa.

Strengthening WC appears to have affected eastern African aridity beginning at 2.11 Ma. This may have been due to stronger WC decreasing ascending motion (i.e., decreased convection) over the western Indian Ocean. Model and proxy data suggest that increased precipitation for eastern Africa is associated with weaker WC and anomalously rising air in the western Indian Ocean (Tierney et al., 2015), such as during some inter-annual El Niño and positive IOD events (Nicholson, 2017). If the Pliocene was indeed characterized by a "permanent" El Niño-like climate, then the changeover to stronger WC in the Early Pleistocene may have disrupted the permanency of rising air over a more humid western Indian Ocean and reduced the influence of these wetter conditions on continental rainfall in easternmost equatorial Africa (Di Nezio et al., 2016).

4.2. Interannual climate variability

Monsoonal rainfall over modern eastern Africa has relationships with interannual climate events that manifest across the Indian Ocean Basin (King et al., 2021; King and Washington, 2021; Nicholson, 2017; Yang et al., 2015). However, there has been much debate about how these relationships evolved through the Plio-Pleistocene and were influenced by tropical SST variability (Scroxton et al., 2011; Tierney et al., 2019; White and Ravelo, 2020; Zhang et al., 2014). In the Indian Ocean, rainfall amounts and WC strength are strongly correlated to the Indian Ocean Dipole (IOD) mode (Mohtadi et al., 2017; Saji et al., 1999). For the western Indian Ocean, model and proxy data predict increased rainfall over eastern Africa during positive IOD events that are concomitant with weaker WC and warmer SST (Tierney et al., 2015). Large floods in tropical eastern Africa occur with weaker Indian Ocean WC and positive IOD (Cai et al., 2013). Other studies suggest changing WC intensity evokes a more variable hydroclimate response over Africa and the western Indian Ocean (Mohtadi et al., 2017; Saji and Yamagata, 2003).

The interplay between the IOD mode and orbital climatic precession is predicted to modulate tropical rainfall variability over northeast Africa (Johnson et al., 2016). Our EHA model (Fig. 5) suggests increased precessional amplitudes through strengthening WC, which may signal a change in interannual IOD behavior (Caley et al., 2018). Other Turkana Basin records from studies of lake outcrops and cores also demonstrate increasing precessional variability and abrupt climate changes through strengthening WC (Joordens et al., 2011; Lupien et al., 2020; Yost et al., 2021). However, these lake records do not show the shift towards a drier monsoon at 2.11–1.66 Ma like our $\delta^{18}O_{PC}$ record. Part of this discrepancy may be because the sources of the paleo-lake water are exotic rivers that have catchments ~300–700 km away from the present-day lake. These sources are at highlands and escarpments that have humid climate settings unlike the semi-arid Lake Turkana region. The climate and topographic patterns in Fig. 1A reflect a rainfall difference of >1500 mm/yr between Turkana and the Ethiopian highlands source area of its largest inflow river (Nicholson, 2017; Yang et al., 2015). Our $\delta^{18}O_{PC}$ record is derived from paleosols and thus registers proximal climate information. The lake records may suggest the distal source areas of Lake Turkana water were buffered from the aridification associated with WC intensification.

4.3. Paleoenvironmental change and human origins

In the Turkana Basin and Lower Omo Valley, paleoclimate proxy records show general agreement with our $\delta^{18}O_{PC}$ compilation, suggesting climatic drying at 2.11–1.66 Ma because of stronger WC. Fossil bovid abundances document an increase in Alcelaphini, Antilopini, and Hippotragini proportions relative to the total bovid population circa 2.0 Ma, indicating increased aridity and the development of seasonally dry grasslands, bushlands, and woodland-grassland mosaics (Bobe et al., 2007). Similarly, (Paquette and Drapeau, 2021) assessed the Omo Group's faunal enamel $\delta^{18}O$ values in several temporal bins and interpreted increasing aridity across three intervals: 2.4–1.9 Ma, 1.9–1.5 Ma, and 1.5–1.3 Ma, in agreement with our directional $\delta^{18}O_{PC}$ trend. However, other isotopic proxy records suggest that human evolution in eastern Africa occurred in absence of major hydroclimate change at ~2.0 Ma (Blumenthal et al., 2017; Passey et al., 2010; Polissar et al., 2019). These isotopic records may be in disagreement because of low sampling resolution and thus may not be registering the climate change [see also comment by (Schefuß and Dupont, 2020)]. For example, the aridity index study (Blumenthal et al., 2017) utilized a faunal enamel $\delta^{18}O$-based aridity index and found fluctuating water deficits from 4 to 0 Ma across several eastern African locales but no directional aridity trend. This contrasts our $\delta^{18}O_{PC}$ record but, importantly, the conclusions of the aridity index study are based upon only eight observations for the ~3.6 Myr duration of the Omo Group.

The spread of C_4 grasslands during the Plio-Pleistocene in eastern Africa has been linked to the concomitant increase of mammalian C_4-grazer speciosity (Cerling et al., 2015; Faith et al., 2018) and adaptive milestones in hominin evolution (Cerling et al., 2011). Low atmospheric pCO_2 concentration and heightened aridity both promote the spread of C_4 grasslands relative to woody vegetation structures (Bond et al., 2003; Ehleringer et al., 1997; Sankaran et al., 2005), but debate surrounds what were the environmental drivers of African vegetation change during Mio-Pleistocene hominin evolution (Blumenthal et al., 2017; Faith et al., 2018; Passey et al., 2010; Polissar et al., 2019; Schefuß and Dupont, 2020). To address this, (Quinn and Lepre, 2021) compiled several $\delta^{13}C_{PC}$ datasets from the East African Rift System and found a major shift towards higher abundances of C_4 vegetation circa 2.0 Ma (**Fig. S1**). We assessed these published $\delta^{13}C_{PC}$ data from the Omo Group

with spectral analysis and derived results (**Fig. S2**) that differed from the orbital climate forcing carried by the $\delta^{18}O_{PC}$ record (Fig. 4). The 2π MTM and Blackman-Tukey results for the $\delta^{13}C_{PC}$ time series failed to indicate long orbital eccentricity with power or significance, and the climatic precession had weaker MTM expression as compared to the $\delta^{18}O_{PC}$ record. However, short orbital eccentricity had power and marginally lower (95%) significance according to MTM and was considered significant by Blackman-Turkey results (**Fig. S2**). Vegetation structures are sensitive to several factors other than climate such as herbivore feeding ecology, fire, and atmospheric pCO_2 (Sankaran et al., 2005). Thus, changes need not mirror the $\delta^{18}O_{PC}$ record, which is more attuned to rainfall and evaporation. Furthermore, African vegetation may respond nonlinearly to orbital insolation forcing (deMenocal et al., 2000) (Shanahan et al., 2015). The nonlinearity may distort the registration of the climate sine wave to the paleoenvironmental record thereby impeding the signal detection. We suggest that among other factors, climatic drying beginning near 2.11 Ma likely contributed to increasing C_4 vegetation abundance and a loss of woody cover in the Turkana region.

Changing C_3 and C_4 floral communities influenced by paleoclimatic drying produced a variety of vegetation mosaics within the Turkana region (Bonnefille, 1995; Cerling et al., 2011; Feakins et al., 2013; Levin et al., 2011; Wynn, 2004), which likely influenced hominin diets. Enamel $\delta^{13}C$ data indicate that early Pleistocene Turkana hominins partitioned the C_3-C_4 mixed feeding omnivore dietary niche (Cerling et al., 2013). Members of genus *Homo* (e.g., *Homo habilis*, *Homo rudolfensis*) maintained their C_3-C_4 omnivory, whereas *Paranthropus boisei* evolved to be a C_4 plant specialist (Cerling et al., 2013; Martin et al., 2020; Wynn et al., 2020). Several lines of evidence (morphology, caloric requirements, cutmarked fauna, lithic assemblages) imply that *Homo erectus* engaged in a higher level of faunivory than other sympatric hominins potentially through carcass scavenging or hunting (Pobiner et al., 2008; Toth and Schick, 2019). Dietary niche partitioning may have been influenced by dietary competition, largely entailing exclusion of *P. boisei* from the C_3-C_4-mixed feeding omnivorous niche by members of *Homo* (Quinn and Lepre, 2021). Secondary productivity likely increased with higher abundances of C_4-dominated vegetation structures (Leonard et al., 2003), giving rise to a greater number of herbivore ungulates for *Homo erectus* to exploit while *P. boisei* seemingly focused on the abundant C_4 plants.

Fig. 10 represents a best estimate of the timing of the major hominin taxa and first appearances for stone tool material cultures that are constrained by our Plio-Pleistocene study interval of 4.33 to 0.65 Ma (see also **Table S3**). We acknowledge that the Omo Group sedimentary formations under consideration only represent one area of Africa where hominin fossils and archaeological sites have been discovered. Notably, there are a number of significant localities known from the northwest (Hublin et al., 2017) and southern (Berger et al., 2010) parts of the continent, and Sahara/Sahel (Brunet et al., 2002) finds that demonstrate hominin evolution was more widespread that just the rift valley of eastern Africa. Important sites throughout Ethiopia (Alemseged et al., 2006; Haile-Selassie et al., 2015; White et al., 2006), Olduvai Gorge in Tanzania (Blumenschine et al., 2003; Mercader et al., 2021), and fossils from Malawi (Schrenk et al., 1993) contribute substantially to our understanding of human origins. However, the paleoanthropology record of the Turkana Basin is renowned for its breadth of fossils showing Plio-Pleistocene hominin biodiversity (Wood and Leakey, 2011).

Early Pliocene sediments of the Turkana Basin have yielded numerous body fossils of *Australopithecus anamensis*, which provides important evidence to constrain the origins of habitual bipedality in the hominin lineage (Leakey et al., 1995). Dated tuffaceous horizons in the Kanapoi Formation bracket a majority of the fossil-bearing levels to between about 4.2 and 4.1 Ma (Leakey et al., 1998). Other *Australopithecus*-like fossils within the Nachukui and Shungura formations may have affinities with *A. afarensis* but this is an ongoing debate (Brown et al., 2013; Ward et al., 1999; Wood and Boyle, 2016).

Archaeological investigations have yielded the oldest stone tools in the world yet known from the Lomekwi Member of the Nachukui Formation. The stone tool artifacts were recovered in-situ from sediments that accumulated during the Mammoth Subchron and date to 3.3–3.2 Ma (Harmand et al., 2015). Nearby sedimentary strata have yielded the

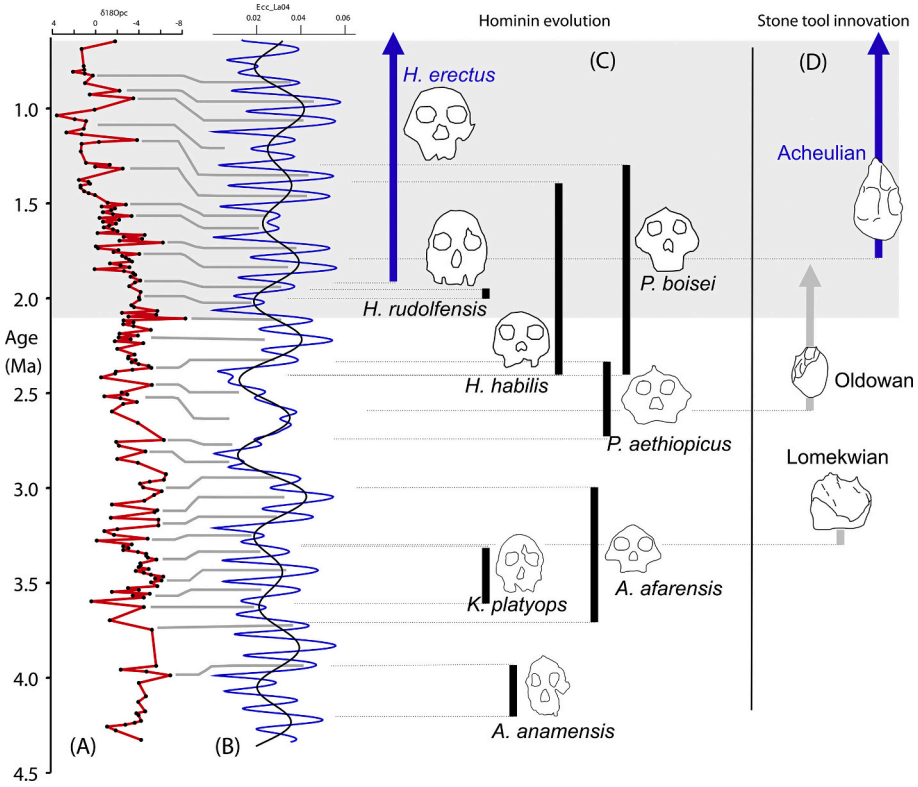

Fig. 10. Paleoclimate context of human origins. (A) Chronology of hydroclimate changes indicated by $\delta^{18}O_{PC}$ spectral analyses and chronostratigraphic correlations with the marine core data. Most of the variability of the $\delta^{18}O_{PC}$ time series lies with eccentricity, suggesting short and long eccentricity insolation forcing of monsoonal rainfall. (B) long and short eccentricity as in Fig. 6. (C) Temporal ranges of hominin species and (D) age estimates for the origins of stone tool traditions from northwest Kenya and southwest Ethiopia. Gray box symbolizes the onset of a long-term directional change towards a drier paleoclimate that perhaps was accompanied by increased short-term climatic variability, interpreted to have selected for *H. erectus*, Acheulian stone tools, and a culling of Early Pleistocene hominin taxonomic diversity. This climate change at 2.11 Ma is attributed to stronger Walker Circulation. Thin horizontal lines correlate hominin and stone tool events to positions within the astronomical curves.

cranial fossil of *Kenyanthropus platyops* (Leakey et al., 2001), which is a somewhat idiosyncratic hominin that might have been the manufacturer of the tools. Higher in the section, one of the oldest known specimens of the genus *Paranthropus* (Walker et al., 1986) was excavated from sands that lie beneath the Lokalalei Tuff dated to ~2.53 Ma (McDougall et al., 2012).

Adjacent to the Lomekwi archaeological site, is the site complex of Kokiselei, which preserves both the developed Oldowan and Acheulian artifacts (Roche et al., 2003). Notably, Kokiselei 4 (KS4) has a stratigraphic position that is situated just above a normal to reverse paleomagnetic reversal correlated to upper Olduvai and lower Matuyama transition at ~1.8 Ma, making KS4 one of the oldest Acheulian sites in the world (Beyene et al., 2013; Lepre et al., 2011). Acheulian tools are argued to be primarily made by *Homo erectus* for large animal carcass processing (Toth and Schick, 2019).

On the east side of Lake Turkana, the Koobi Fora Formation has provided evidence for the taxonomic diversity within early *Homo* hypodigm dated to about 2.0–1.5 Ma. Important partial crania of *H. habilis* and *H. rudolfensis* have stratigraphic positions in close proximity to the level of the KBS Tuff (Leakey et al., 2012), which is dated to 1.87 ± 0.02 Ma (McDougall et al., 2012). The global first appearance datum of *H. erectus* is thought to be the partial neurocranium of a juvenile (DNH 134) from South Africa that dates to 2.0 Ma (Herries et al., 2020). The next oldest is the occipital fragment KNM-ER 2598 from Koobi Fora that lies below the KBS Tuff and thus date to 1.9 Ma (Antón et al., 2014; Feibel et al., 1989; Hammond et al., 2021; Lepre and Kent, 2010, 2015; Wood and Leakey, 2011). In addition, the Koobi Fora Formation has produced the oldest known near complete cranium of an adult African *H. erectus* (KNM-ER 3733) that is dated to about 1.6 Ma (Lepre and Kent, 2015). This specimen is penecontemporaneous with stone tool artifacts of the developed Oldowan of the Koobi Fora Formation (Mana et al., 2019) that derive from the Okote Member. Lastly, Chari Member specimens of *H. habilis* are some of the geologically youngest known and may indicate that the extinction of this species occurred between 1.5 and 1.4 Ma (Spoor et al., 2007).

Variability Selection Hypothesis (Potts, 1998; Potts and Faith, 2015) links hominin first and last appearance datums (FAD/LAD) to the maxima of the long eccentricity cycle, predicting that climate conditions associated with insolation changes every 405 kyr increased habitat variability (deMenocal, 2004; Maslin et al., 2014; Potts and Faith, 2015; Trauth et al., 2009). However, as shown in Fig. 10, there appears to be no consistent temporal correlation between the FAD/LAD and long eccentricity maxima. This interpretation, for example, is clearly the case for the oldest stone tools in the world yet known, discovered at Lomekwi in the Turkana Basin and dated to 3.3–3.2 Ma (Harmand et al., 2015). Isotopic data in Fig. 7 come directly from the stone tool site and when coupled with the other data demonstrate that the stone tools at 3.3 Ma are associated with eccentricity amplitudes decreasing towards a long eccentricity minimum. Similarly, the interval at 2.5–3.0 Ma is characterized by some of the lowest short eccentricity amplitudes for the entire study interval (Fig. 6). Such low eccentricity suggests weak modulation of precessional insolation delivered to eastern Africa, and less seasonality for monsoonal rainfall (Rossignol-Strick et al., 1982). The timeframe of 2.5–3.0 Ma witnessed the rise of Oldowan stone tools (Semaw et al., 1997), constrains the oldest paranthropine fossil currently known (Wood and Constantino, 2007), and probably is when the genus *Homo* originated (DiMaggio et al., 2015). The weak eccentricity modulation of the African monsoon suggests hominin originations at 2.5–3.0 Ma occurred within a setting of low climatic variability.

No taxon appears to endure for more than about two 405-kyr eccentricity cycles before going extinct (Fig. 10), suggesting that early hominins as a lineage of primates may have been poorly adapted to environmental variability at this long orbital time scale. The exception, however, is *H. erectus*. This large-brained and -bodied ancestor to later *Homo* is hypothesized to have been well adapted to variable environments, evident from its wide geographic and ecological distribution through most of tropical Africa and Asia (Antón et al., 2014). In eastern Africa, the first appearance datum of *H. erectus* and Acheulian stone tools co-occur with strengthening WC, directional climatic drying, and perhaps more short-term climate variability—particularly on the interannual time scale. Interannual climate events, like El Niño or the IOD mode, went through changes in intensity and recurrence frequency during strengthening WC strength (Mohtadi et al., 2017; White and Ravelo, 2020). The recurrence frequency of extreme interannual rainfall events correlated to positive IOD modes varies by a factor of almost three during global warming/cooling phases (Cai et al., 2014). Beginning near 2.11 Ma, we suggest that similar variations to short-term climate changes may have been cooccurring with the direction climatic drying indicated by the $\delta^{18}O_{PC}$ (Fig. 3B). In eastern Africa, *H. erectus* appears to have been the only hominin well adapted for this new setting of directional climatic drying coupled with short-term environmental variability, as the genus *Homo* was culled to one species by ~1.5 Ma and paranthropines of eastern Africa went extinct at 1.5–1.0 Ma (Fig. 10).

5. Summary and conclusions

Multidisciplinary studies over the last decade have provided a more detailed understanding of paleoclimate and human origins in eastern Africa. However, it has been a challenge to recover long-term records (>1 Myr) that can be used to demonstrate orbital climate forcing and assess directional climate shifts through the Plio-Pleistocene. To address this problem, we constructed a ~ 3.6 Myr (4.33–0.65 Ma) stable oxygen isotope record from pedogenic carbonate nodules ($\delta^{18}O_{PC}$) collected from the radiometrically-dated Omo Group outcrops in Kenya and Ethiopia. This $\delta^{18}O_{PC}$ record is noteworthy not only for its length and age constraints, but also because it was derived from some of the most important archaeological and hominin fossil sites currently known. This allows us to directly interpret the terrestrial paleoenvironments where hominins lived and to compare the changes to turning points in Plio-Pleistocene global climate and paleoceanographic events across the Indo-Pacific equatorial tropics.

The $\delta^{18}O_{PC}$ record from the Omo Group reveals rainfall/evaporation conditions indicative of climate. Some of the $\delta^{18}O_{PC}$ variation observed may be attributed to other controls, such as paleogeographic context (Levin et al., 2011; Quinn et al., 2007); however, spectral analysis and chronostratigraphic comparisons with astronomical solutions indicate that the $\delta^{18}O_{PC}$ variability provides a record of orbital climate forcing from eccentricity, with some intervals demonstrating amplitude modulation of short eccentricity (~100 kyr) cycles.

This $\delta^{18}O_{PC}$ record also indicates a shift towards a drier climate beginning at 2.11 Ma, which correlates to a thickening mixed layer in the eastern Indian Ocean and marine upwelling events in the eastern Pacific Ocean (Bali et al., 2020; Lawrence et al., 2006). These paleoceanographic changes are related to strengthening Walker Circulation, implying that the climatic drying in eastern Africa was part of a larger transformation of the equatorial tropics, characterized by new SST gradients and ocean-atmospheric circulation patterns. Evolutive harmonics analysis of the $\delta^{18}O_{PC}$ time series demonstrated increased significance for climatic precession at ~2.5–1.7 Ma, which may be indicative of the eastern African rainfall experiencing more interannual variability through stronger Walker Circulation.

At 1.9–1.8 Ma, *Homo erectus* and Acheulian stone tools first appear in eastern Africa during directional climatic drying. Other temporally long stable isotope records suggest an unchanging hydroclimate during Plio-Pleistocene evolutionary events (Blumenthal et al., 2017; Polissar et al., 2019). However, these records lack the resolution to demonstrate orbital-scale changes in the data, especially through key climatic and biotic intervals. In contrast, our interpretation of directional climatic drying starting at 2.11 Ma is deduced from a $\delta^{18}O$ record of orbital climate change. If higher frequency $\delta^{18}O_{PC}$ changes are due to orbital climate forcing, then the simplest explanation is that the long-term shift

in the record is also due to climate change. These other isotopic studies demonstrating no hydroclimate changes are based on floral and fauna taxa that were sensitive to multiple drivers of ecological change other than climate. Such is probably the case for the pedogenic carbon isotope ($\delta^{13}C_{PC}$) vegetation record for our study area responding to several influences in addition to climate, including pCO_2, substrate and hydrological configuration, herbivore community diets, interspecific competition, among others. The $\delta^{13}C_{PC}$ data showed weaker indications of orbital climate forcing as compared to the $\delta^{18}O_{PC}$ record, but indicated a shift towards higher abundances of C_4 vegetation at ~2.0 Ma, consistent with heightened aridity.

The Plio-Pleistocene $\delta^{18}O_{PC}$ composition of Omo Group paleosols appears to be strongly influenced by orbital insolation forcing of monsoonal rainfall. Superimposed upon the orbital trends was a drying response to stronger Walker Circulation. However, there appears to be no clear indication that the Plio-Pleistocene intensification of Northern Hemisphere glaciation was responsible for either climate cycles or an abrupt, stepwise shifts in the $\delta^{18}O$ record, like observed in marine records of African dust flux (deMenocal, 2004). A common mechanism to explain paleoclimate change in eastern Africa is the latitudinal constriction of tropical convergence and the associated pole-equator temperature gradient induced by the expansion of polar ice sheets (Caley et al., 2018; Maslin and Trauth, 2009). Rainfall over northwest Kenya and southeast Ethiopia appears to have been unaffected by such meridional movement of the tropical rain belt and buffered from changes to trade wind intensities and Atlantic SST temperatures developed during earliest Pleistocene glacial activity.

Declaration of Competing Interest

The authors have no known competing interests that influenced the study.

Acknowledgements

Authorization for conducting scientific research in Kenya was permitted by the National Council for Science and Technology and gratitude is extended to the Office of the President of Kenya and the Ministry of Education, Science and Technology. Research affiliation was kindly provided by the National Museums of Kenya, and Drs. Mzalendo Kibunjia, Purity Kiura, and Kyalo Manthi are thanked for their ongoing support of the research. The Turkana Basin Institute, West Turkana Archaeological Project, and Kenya Wildlife Services are acknowledged for logistical support while conducting fieldwork. All of the new isotopic measurements reported in this paper were conducted at the Stable Isotope Laboratory of Earth and Planetary Sciences, Rutgers University, under the auspices of James Wright and Richard Mortlock. Craig Feibel is thanked for his introduction to the Lake Turkana region. Two anonymous reviewers greatly improved the submitted draft of this manuscript through their criticisms and suggestions. Funding was provided by National Science Foundation grants BCS-1818805 (CJL) and BCS-1455274 (RLQ).

Appendix A. Supplementary data

Supplementary data to this article can be found online at https://doi.org/10.1016/j.gloplacha.2021.103684.

References

Alemseged, Z., Spoor, F., Kimbel, W.H., Bobe, R., Geraads, D., Reed, D., Wynn, J.G., 2006. A juvenile early hominin skeleton from Dikika, Ethiopia. Nature 443, 296–301. https://doi.org/10.1038/nature05047.

Amundson, R.G., Wang, Y., 1996. The relationship between the oxygen isotopic composition of soil CO_2 and soil water. IAEA, Isotopes Water Resour. Manage. 315–332.

Antón, S.C., Potts, R., Aiello, L.C., 2014. Evolution of early *Homo*: an integrated biological perspective. Science 345, 1236828. https://doi.org/10.1126/science.1236828.

Bali, H., Gupta, A.K., Mohan, K., Thirumalai, K., Tiwari, S.K., Panigrahi, M.K., 2020. Evolution of the Oligotrophic West Pacific warm pool during the Pliocene-Pleistocene boundary. Paleoceanogr. Paleoclimatol. 35 https://doi.org/10.1029/2020PA003875.

Berger, L.R., de Ruiter, D.J., Churchill, S.E., Schmid, P., Carlson, K.J., Dirks, P.H.G.M., Kibii, J.M., 2010. *Australopithecus sediba*: a new species of *Homo*-like Australopith from South Africa. Science 328, 195–204. https://doi.org/10.1126/science.1184944.

Beyene, Y., Katoh, S., WoldeGabriel, G., Hart, W.K., Uto, K., Sudo, M., Kondo, M., Hyodo, M., Renne, P.R., Suwa, G., Asfaw, B., 2013. The characteristics and chronology of the earliest Acheulean at Konso, Ethiopia. Proc. Natl. Acad. Sci. 110, 1584–1591. https://doi.org/10.1073/pnas.1221285110.

Birkeland, P.W., 1984. Soils and Geomorphology. Oxford University Press, New York.

Blumenschine, R.J., Peters, C.R., Fidelis, M.T., Clarke, R.J., Deino, A.L., Hay, R.L., Swisher, C.C., Stanistreet, I.G., Ashley, G.M., McHenry, L.J., Sikes, N.E., van der Merwe, N.J., Tactikos, J.C., Cushing, A.E., Deocampo, D.M., Njau, J.K., Ebert, J.I., 2003. Late Pliocene *Homo* and hominid land use from Western Olduvai Gorge, Tanzania. Science 299, 1217–1221. https://doi.org/10.1126/science.1075374.

Blumenthal, S.A., Levin, N.E., Brown, F.H., Brugal, J.-P., Chritz, K.L., Harris, J.M., Jehle, G.E., Cerling, T.E., 2017. Aridity and hominin environments. Proc. Natl. Acad. Sci. U. S. A. 114, 7331–7336. https://doi.org/10.1073/pnas.1700597114.

Bobe, R., Behrensmeyer, A.K., Eck, G.G., Harris, J.M., 2007. Patterns of abundance and diversity in late Cenozoic bovids from the Turkana and Hadar Basins, Kenya and Ethiopia. In: Bobe, R., Alemseged, Z., Behrensmeyer, A.K. (Eds.), Hominin Environments in the East African Pliocene: An Assessment of the Faunal Evidence, Vertebrate Paleobiology and Paleoanthropology Series. Springer Netherlands, Dordrecht, pp. 129–157. https://doi.org/10.1007/978-1-4020-3098-7_6.

Boës, X., Prat, S., Arrighi, V., Feibel, C., Haileab, B., Lewis, J., Harmand, S., 2019. Lake-level changes and hominin occupations in the arid Turkana basin during volcanic closure of the Omo River outflows to the Indian Ocean. Quat. Res. 91, 892–909. https://doi.org/10.1017/qua.2018.118.

Bond, W.J., Midgley, G.F., Woodward, F.I., 2003. The importance of low atmospheric CO_2 and fire in promoting the spread of grasslands and savannas. Glob. Chang. Biol. 9, 973–982. https://doi.org/10.1046/j.1365-2486.2003.00577.x.

Bonnefille, R., 1995. A reassessment of the Plio-Pleistocene pollen record of East Africa. In: Vrba, E.S., Denton, G.H., Partridge, T.C., Burckle, L.H. (Eds.), Paleoclimate and Evolution, with Emphasis on Human Origins. Yale University Press, New Haven, pp. 299–310.

Breecker, D.O., Sharp, Z.D., McFadden, L.D., 2009. Seasonal bias in the formation and stable isotopic composition of pedogenic carbonate in modern soils from Central New Mexico, USA. Geol. Soc. Am. Bull. 121, 630–640. https://doi.org/10.1130/B26413.1.

Brown, F.H., 1995. The potential of the Turkana Basin for paleoclimatic reconstruction in East Africa. In: Vrba, E.S., Denton, G.H., Patridge, T.C., Burckle, L.H. (Eds.), Paleoclimate and Evolution with Emphasis on Human Origins. Yale University Press, New Haven, pp. 319–330.

Brown, F.H., Feibel, C.S., 1991. Stratigraphy, depostional environments, and palaeogeography of the Koobi Fora Formation. Koobi Fora Research Project: Stratigraphy, Artiodactyls, and Palaeoenvironments, vol. 3. Claredon Press, Oxford, pp. 1–30.

Brown, F.H., McDougall, I., Gathogo, P.N., 2013. Age ranges of *Australopithecus* species, Kenya, Ethiopia, and Tanzania. In: Reed, K.E., Fleagle, J.G., Leakey, R.E. (Eds.), The Paleobiology of *Australopithecus*. Springer Netherlands, Dordrecht, pp. 7–20.

Brunet, M., Guy, F., Pilbeam, D., Mackaye, H.T., Likius, A., Ahounta, D., Beauvilain, A., Blondel, C., Bocherens, H., Boisserie, J.-R., De Bonis, L., Coppens, Y., Dejax, J., Denys, C., Duringer, P., Eisenmann, V., Fanone, G., Fronty, P., Geraads, D., Lehmann, T., Lihoreau, F., Louchart, A., Mahamat, A., Merceron, G., Mouchelin, G., Otero, O., Campomanes, P.P., De Leon, M.P., Rage, J.-C., Sapanet, M., Schuster, M., Sudre, J., Tassy, P., Valentin, X., Vignaud, P., Viriot, L., Zazzo, A., Zollikofer, C., 2002. A new hominid from the Upper Miocene of Chad, Central Africa. Nature 418, 145–151. https://doi.org/10.1038/nature00879.

Cai, W., Zheng, X.-T., Weller, E., Collins, M., Cowan, T., Lengaigne, M., Yu, W., Yamagata, T., 2013. Projected response of the Indian Ocean Dipole to greenhouse warming. Nat. Geosci. 6, 999–1007. https://doi.org/10.1038/ngeo2009.

Cai, W., Santoso, A., Wang, G., Weller, E., Wu, L., Ashok, K., Masumoto, Y., Yamagata, T., 2014. Increased frequency of extreme Indian Ocean Dipole events due to greenhouse warming. Nature 510, 254–258. https://doi.org/10.1038/nature13327.

Caley, T., Extier, T., Collins, J.A., Schefuß, E., Dupont, L., Malaizé, B., Rossignol, L., Souron, A., McClymont, E.L., Jimenez-Espejo, F.J., García-Comas, C., Eynaud, F., Martinez, P., Roche, D.M., Jorry, S.J., Charlier, K., Wary, M., Gourves, P.-Y., Billy, I., Giraudeau, J., 2018. A two-million-year-long hydroclimatic context for hominin evolution in southeastern Africa. Nature 560, 76–79. https://doi.org/10.1038/s41586-018-0309-6.

Campisano, C.J., Cohen, A.S., Arrowsmith, J.R., Asrat, A., Behrensmeyer, A.K., Brown, E. T., Deino, A.L., Deocampo, D.M., Feibel, C.S., Kingston, J.D., Lamb, H.F., Lowenstein, T.K., Noren, A., Olago, D.O., Owen, R.B., Pelletier, J.D., Potts, R., 2017. The Hominin Sites and Paleolakes Drilling Project: High-Resolution Paleoclimate Records from the East African Rift System and Their Implications for Understanding the Environmental Context of Hominin Evolution. PaleoAnthropology 1–43. https://doi.org/10.4207/PA.2017.ART104. PaleoAnthropology Society.

Cane, M.A., Molnar, P., 2001. Closing of the Indonesian seaway as a precursor to east African aridification around 3–4 million years ago. Nature 411, 157–162. https://doi.org/10.1038/35075500.

Cerling, T.E., 1984. The stable isotopic composition of modern soil carbonate and its relationship to climate. Earth Planet. Sci. Lett. 71, 229–240. https://doi.org/10.1016/0012-821X(84)90089-X.

Cerling, T.E., Bowman, J.R., O'Neil, J.R., 1988. An isotopic study of a fluvial-lacustrine sequence: the Plio-Pleistocene Koobi Fora sequence, East Africa. Palaeogeogr. Palaeoclimatol. Palaeoecol. 63, 335–356. https://doi.org/10.1016/0031-0182(88)90104-6.

Cerling, T.E., Quade, J., 1993. Stable Carbon and Oxygen Isotopes in Soil Carbonates. In: Swart, P.K., Lohmann, K.C., Mckenzie, J., Savin, S. (Eds.), Geophysical Monograph Series: Climate Change in Continental Isotopic Records, vol. 78. American Geophysical Union, Washington, D.C., pp. 217–231

Cerling, T.E., Wynn, J.G., Andanje, S.A., Bird, M.I., Korir, D.K., Levin, N.E., Mace, W., Macharia, A.N., Quade, J., Remien, C.H., 2011. Woody cover and hominin environments in the past 6 million years. Nature 476, 51–56. https://doi.org/10.1038/nature10306.

Cerling, T.E., Manthi, F.K., Mbua, E.N., Leakey, L.N., Leakey, M.G., Leakey, R.E., Brown, F.H., Grine, F.E., Hart, J.A., Kaleme, P., Roche, H., Uno, K.T., Wood, B.A., 2013. Stable isotope-based diet reconstructions of Turkana Basin hominins. Proc. Natl. Acad. Sci. 110, 10501–10506. https://doi.org/10.1073/pnas.1222568110.

Cerling, T.E., Andanje, S.A., Blumenthal, S.A., Brown, F.H., Chritz, K.L., Harris, J.M., Hart, J.A., Kirera, F.M., Kaleme, P., Leakey, L.N., Leakey, M.G., Levin, N.E., Manthi, F.K., Passey, B.H., Uno, K.T., 2015. Dietary changes of large herbivores in the Turkana Basin, Kenya from 4 to 1 Ma. Proc Natl Acad Sci USA 112, 11467–11472. https://doi.org/10.1073/pnas.1513075112.

Cohen, A., Campisano, C., Arrowsmith, R., Asrat, A., Behrensmeyer, A.K., Deino, A., Feibel, C., Hill, A., Johnson, R., Kingston, J., Lamb, H., Lowenstein, T., Noren, A., Olago, D., Owen, R.B., Potts, R., Reed, K., Renaut, R., Schäbitz, F., Tiercelin, J.-J., Trauth, M.H., Wynn, J., Ivory, S., Brady, K., Grady, R., Rodysill, J., Githiri, J., Russell, J., Foerster, V., Dommain, R., Rucina, S., Deocampo, D., Russell, J., Billingsley, A., Beck, C., Dorenbeck, G., Dullo, L., Feary, D., Garello, D., Gromig, R., Johnson, T., Junginger, A., Karanja, M., Kimburi, E., Mbuthia, A., McCartney, T., McNulty, E., Muiruri, V., Nambiro, E., Negash, E.W., Njagi, D., Wilson, J.N., Rabideaux, N., Raub, T., Sier, M.J., Smith, P., Urban, J., Warren, M., Yadeta, M., Yost, C., Zinaye, B., 2016. The Hominin Sites and Paleolakes Drilling Project: inferring the environmental context of human evolution from eastern African rift lake deposits. Sci. Drill. 21, 1–16. https://doi.org/10.5194/sd-21-1-2016.

Deckers, J., Spaargaren, O., Nachtergaele, F., 2001. Vertisols: Genesis, Properties and Soilscape Management for Sustainable Development. In: Syers, J.K., Penning de Vries, F.W.T., Nyamudeza, P. (Eds.), The Sustainable Management of Vertisols. CABI, New York, pp. 3–20.

deMenocal, P.B., 2004. African climate change and faunal evolution during the Pliocene–Pleistocene. Earth Planet. Sci. Lett. 220, 3–24. https://doi.org/10.1016/S0012-821X(04)00003-2.

deMenocal, P., Ortiz, J., Guilderson, T., Adkins, J., Sarthein, M., Baker, L., Yarusinsky, M., 2000. Abrupt onset and termination of the African Humid Period: rapid climate responses to gradual insolation forcing. Quaternary Science Reviews 19, 347–361. Pergamon.

Deocampo, D.M., Berry, P.A., Beverly, E.J., Ashley, G.M., Jarrett, R.E., 2017. Whole-rock geochemistry tracks precessional control of Pleistocene lake salinity at Olduvai Gorge, Tanzania: a record of authigenic clays. Geology G38950, 1. https://doi.org/10.1130/G38950.1.

Di Nezio, P.N., Timmermann, A., Tierney, J.E., Jin, F., Otto-Bliesner, B., Rosenbloom, N., Mapes, B., Neale, R., Ivanovic, R.F., Montenegro, A., 2016. The climate response of the Indo-Pacific warm pool to glacial sea level. Paleoceanography 31, 866–894. https://doi.org/10.1002/2015PA002890.

DiMaggio, E.N., Campisano, C.J., Rowan, J., Dupont-Nivet, G., Deino, A.L., Bibi, F., Lewis, M.E., Souron, A., Garello, D., Werdelin, L., Reed, K.E., Arrowsmith, J.R., 2015. Late Pliocene fossiliferous sedimentary record and the environmental context of early *Homo* from Afar, Ethiopia. Science 347, 1355–1359. https://doi.org/10.1126/science.aaa1415.

DiNezio, P.N., Tierney, J.E., 2013. The effect of sea level on glacial Indo-Pacific climate. Nat. Geosci. 6, 485–491. https://doi.org/10.1038/ngeo1823.

DiNezio, P.N., Tierney, J.E., Otto-Bliesner, B.L., Timmermann, A., Bhattacharya, T., Rosenbloom, N., Brady, E., 2018. Glacial changes in tropical climate amplified by the Indian Ocean. Sci. Adv. 4, eaat9658. https://doi.org/10.1126/sciadv.aat9658.

Donges, J.F., Donner, R.V., Trauth, M.H., Marwan, N., Schellnhuber, H.-J., Kurths, J., 2011. Nonlinear detection of paleoclimate-variability transitions possibly related to human evolution. Proc. Natl. Acad. Sci. 108, 20422–20427. https://doi.org/10.1073/pnas.1117052108.

Ehleringer, J.R., Cerling, T.E., Helliker, B.R., 1997. C_4 photosynthesis, atmospheric CO_2, and climate. Oecologia 112, 285–299. https://doi.org/10.1007/s004420050311.

Etourneau, J., Schneider, R., Blanz, T., Martinez, P., 2010. Intensification of the Walker and Hadley atmospheric circulations during the Pliocene–Pleistocene climate transition. Earth Planet. Sci. Lett. 297, 103–110. https://doi.org/10.1016/j.epsl.2010.06.010.

Faith, J.T., Rowan, J., Du, A., Koch, P.L., 2018. Plio-Pleistocene decline of African megaherbivores: no evidence for ancient hominin impacts. Science 362, 938–941. https://doi.org/10.1126/science.aau2728.

Feakins, S.J., deMenocal, P.B., Eglinton, T.I., 2005. Biomarker records of late Neogene changes in northeast African vegetation. Geology 33, 977. https://doi.org/10.1130/G21814.1.

Feakins, S.J., Levin, N.E., Liddy, H.M., Sieracki, A., Eglinton, T.I., Bonnefille, R., 2013. Northeast African vegetation change over 12 m.y. Geology 41, 295–298. https://doi.org/10.1130/G33845.1.

Fedorov, A.V., Brierley, C.M., Lawrence, K.T., Liu, Z., Dekens, P.S., Ravelo, A.C., 2013. Patterns and mechanisms of early Pliocene warmth. Nature 496, 43–49. https://doi.org/10.1038/nature12003.

Feibel, C.S., 1999. Basin evolution, sedimentary dynamics and hominid habitats in East Africa: an ecosystem approach. In: Bromage, T.G., Schrenk, F. (Eds.), African Biogeography, Climate Change, and Human Evolution. Oxford University Press, Oxford, pp. 276–281.

Feibel, C.S., Brown, F.H., McDougall, I., 1989. Stratigraphic context of fossil hominids from the Omo group deposits: Northern Turkana Basin, Kenya and Ethiopia. Am. J. Phys. Anthropol. 78, 595–622. https://doi.org/10.1002/ajpa.1330780412.

Ford, H.L., Ravelo, A.C., Dekens, P.S., LaRiviere, J.P., Wara, M.W., 2015. The evolution of the equatorial thermocline and the early Pliocene *El Padre* mean state. Geophys. Res. Lett. 42, 4878–4887. https://doi.org/10.1002/2015GL064215.

Gordon, A.L., Fine, R.A., 1996. Pathways of water between the Pacific and Indian oceans in the Indonesian seas. Nature 379, 146–149. https://doi.org/10.1038/379146a0.

Haile-Selassie, Y., Gibert, L., Melillo, S.M., Ryan, T.M., Alene, M., Deino, A., Levin, N.E., Scott, G., Saylor, B.Z., 2015. New species from Ethiopia further expands Middle Pliocene hominin diversity. Nature 521, 483–488. https://doi.org/10.1038/nature14448.

Hammond, A.S., Mavuso, S.S., Biernat, M., Braun, D.R., Jinnah, Z., Kuo, S., Melaku, S., Wemanya, S.N., Ndiema, E.K., Patterson, D.B., Uno, K.T., Palcu, D.V., 2021. New hominin remains and revised context from the earliest *Homo erectus* locality in East Turkana, Kenya. Nat. Commun. 12, 1939. https://doi.org/10.1038/s41467-021-22208-x.

Harmand, S., Lewis, J.E., Feibel, C.S., Lepre, C.J., Prat, S., Lenoble, A., Boës, X., Quinn, R.L., Brenet, M., Arroyo, A., Taylor, N., Clément, S., Daver, G., Brugal, J.-P., Leakey, L., Mortlock, R.A., Wright, J.D., Lokorodi, S., Kirwa, C., Kent, D.V., Roche, H., 2015. 3.3-million-year-old stone tools from Lomekwi 3, West Turkana, Kenya. Nature 521, 310–315. https://doi.org/10.1038/nature14464.

Harris, J.M., Brown, F.H., Leakey, M.G., 1988. Geology and paleontology of Plio-Pleistocene localities west of Lake Turkana, Kenya. Contrib. Sci., 399 Natural History Museum of Los Angeles County, pp. 1–128.

Herbert, T.D., Peterson, L.C., Lawrence, K.T., Liu, Z., 2010. Tropical ocean temperatures over the past 3.5 million years. Science 328, 1530–1534. https://doi.org/10.1126/science.1185435.

Herries, A.I.R., Martin, J.M., Leece, A.B., Adams, J.W., Boschian, G., Joannes-Boyau, R., Edwards, T.R., Mallett, T., Massey, J., Murszewski, A., Neubauer, S., Pickering, R., Strait, D.S., Armstrong, B.J., Baker, S., Caruana, M.V., Denham, T., Hellstrom, J., Moggi-Cecchi, J., Mokobane, S., Penzo-Kajewski, P., Rovinsky, D.S., Schwartz, G.T., Stammers, R.C., Wilson, C., Woodhead, J., Menter, C., 2020. Contemporaneity of *Australopithecus*, *Paranthropus*, and early *Homo erectus* in South Africa. Science 368. https://doi.org/10.1126/science.aaw7293 eaaw7293.

Hilgen, F.J., 1991. Astronomical calibration of Gauss to Matuyama sapropels in the Mediterranean and implication for the Geomagnetic Polarity Time Scale. Earth Planet. Sci. Lett. 104, 226–244. https://doi.org/10.1016/0012-821X(91)90206-W.

Hsieh, J.C.C., Chadwick, O.A., Kelly, E.F., Savin, S.M., 1998. Oxygen isotopic composition of soil water: quantifying evaporation and transpiration. Geoderma 82, 269–293. https://doi.org/10.1016/S0016-7061(97)00105-5.

Hublin, J.-J., Ben-Ncer, A., Bailey, S.E., Freidline, S.E., Neubauer, S., Skinner, M.M., Bergmann, I., Le Cabec, A., Benazzi, S., Harvati, K., Gunz, P., 2017. New fossils from Jebel Irhoud, Morocco and the pan-African origin of *Homo* sapiens. Nature 546, 289–292. https://doi.org/10.1038/nature22336.

Jakob, K.A., Ho, S.L., Meckler, A.N., Pross, J., Fiebig, J., Keppler, F., Friedrich, O., 2021. Stable Biological Production in the Eastern Equatorial Pacific across the Plio-Pleistocene transition (~3.35–2.0 Ma). Paleoceanogr. Paleoclimatol. 36. https://doi.org/10.1029/2020PA003965.

Johnson, T.C., Werne, J.P., Brown, E.T., Abbott, A., Berke, M., Steinman, B.A., Halbur, J., Contreras, S., Grosshuesch, S., Deino, A., Scholz, C.A., Lyons, R.P., Schouten, S., Damsté, J.S.S., 2016. A progressively wetter climate in southern East Africa over the past 1.3 million years. Nature 537, 220–224. https://doi.org/10.1038/nature19065.

Joordens, J.C.A., Vonhof, H.B., Feibel, C.S., Lourens, L.J., Dupont-Nivet, G., van der Lubbe, J.H.J.L., Sier, M.J., Davies, G.R., Kroon, D., 2011. An astronomically-tuned climate framework for hominins in the Turkana Basin. Earth Planet. Sci. Lett. 307, 1–8. https://doi.org/10.1016/j.epsl.2011.05.005.

Jung, S.J.A., Davies, G.R., Ganssen, G.M., Kroon, D., 2004. Stepwise Holocene aridification in NE Africa deduced from dust-borne radiogenic isotope records. Earth Planet. Sci. Lett. 221, 27–37. https://doi.org/10.1016/S0012-821X(04)00095-0.

Kang, S.M., Xie, S.-P., Shin, Y., Kim, H., Hwang, Y.-T., Stuecker, M.F., Xiang, B., Hawcroft, M., 2020. Walker circulation response to extratropical radiative forcing. Sci. Adv. 6, eabd3021. https://doi.org/10.1126/sciadv.abd3021.

Kim, S.-T., O'Neil, J.R., 1997. Equilibrium and nonequilibrium oxygen isotope effects in synthetic carbonates. Geochim. Cosmochim. Acta 61, 3461–3475. https://doi.org/10.1016/S0016-7037(97)00169-5.

King, J.A., Washington, R., 2021. Future changes in the Indian Ocean Walker Circulation and Links to Kenyan Rainfall. J. Geophys. Res. Atmos. 126 https://doi.org/10.1029/2021JD034585.

King, J.A., Washington, R., Engelstaedter, S., 2021. Representation of the Indian Ocean Walker circulation in climate models and links to Kenyan rainfall. Int. J. Climatol. 41, E616–E643. https://doi.org/10.1002/joc.6714.

Kodama, K.P., Hinnov, L.A., 2015. Rock Magnetic Cyclostratigraphy, New Analytical Methods in Earth and Environmental Science. Wiley-Blackwell, Chichester, West Sussex, UK.

Laskar, J., Robutel, P., Joutel, F., Gastineau, M., Correia, A.C.M., Levrard, B., 2004. A long-term numerical solution for the insolation quantities of the Earth. Astron. Astrophys. 428, 261–285. https://doi.org/10.1051/0004-6361:20041335.

Lau, K.-M., Yang, S., 2002. Walker Circulation. Encyclopedia of Atmospheric Science. Elsevier, pp. 2505–2510.
Lawrence, K.T., Liu, Z., Herbert, T.D., 2006. Evolution of the Eastern Tropical Pacific through Plio-Pleistocene Glaciation. Science 312, 79–83. https://doi.org/10.1126/science.1120395.
Leakey, M.G., Feibel, C.S., McDougall, I., Walker, A., 1995. New four-million-year-old hominid species from Kanapoi and Allia Bay, Kenya. Nature 376, 565–571. https://doi.org/10.1038/376565a0.
Leakey, M.G., Feibel, C.S., McDougall, I., Ward, C., Walker, A., 1998. New specimens and confirmation of an early age for *Australopithecus anamensis*. Nature 393, 62–66. https://doi.org/10.1038/29972.
Leakey, M.G., Spoor, F., Brown, F.H., Gathogo, P.N., Kiarie, C., Leakey, L.N., McDougall, I., 2001. New hominin genus from eastern Africa shows diverse middle Pliocene lineages. Nature 410, 433–440. https://doi.org/10.1038/35068500.
Leakey, M.G., Spoor, F., Dean, M.C., Feibel, C.S., Antón, S.C., Kiarie, C., Leakey, L.N., 2012. New fossils from Koobi Fora in northern Kenya confirm taxonomic diversity in early *Homo*. Nature 488, 201–204. https://doi.org/10.1038/nature11322.
Leonard, W.R., Robertson, M.L., Snodgrass, J.J., Kuzawa, C.W., 2003. Metabolic correlates of hominid brain evolution. Comp. Biochem. Physiol. Part A 136, 5–15. https://doi.org/10.1016/S1095-6433(03)00132-6.
Lepre, C.J., 2014. Early Pleistocene lake formation and hominin origins in the Turkana–Omo rift. Quat. Sci. Rev. 102, 181–191. https://doi.org/10.1016/j.quascirev.2014.08.012.
Lepre, C.J., 2017. Crevasse-splay and associated depositional environments of the hominin-bearing lower Okote Member, Koobi Fora Formation (Plio-Pleistocene), Kenya. Deposit. Rec. 3, 161–186. https://doi.org/10.1002/dep2.31.
Lepre, C.J., 2019. Constraints on Fe-Oxide Formation in Monsoonal Vertisols of Pliocene Kenya using Rock Magnetism and Spectroscopy. Geochem. Geophys. Geosyst. https://doi.org/10.1029/2019GC008276, 2019GC008276.
Lepre, C.J., Kent, D.V., 2010. New magnetostratigraphy for the Olduvai Subchron in the Koobi Fora Formation, Northwest Kenya, with implications for early *Homo*. Earth Planet. Sci. Lett. 290, 362–374. https://doi.org/10.1016/j.epsl.2009.12.032.
Lepre, C.J., Kent, D.V., 2015. Chronostratigraphy of KNM-ER 3733 and other Area 104 hominins from Koobi Fora. J. Hum. Evol. 86, 99–111. https://doi.org/10.1016/j.jhevol.2015.06.010.
Lepre, C.J., Quinn, R.L., Joordens, J.C.A., Swisher, C.C., Feibel, C.S., 2007. Plio-Pleistocene facies environments from the KBS Member, Koobi Fora Formation: implications for climate controls on the development of lake-margin hominin habitats in the Northeast Turkana Basin (Northwest Kenya). J. Hum. Evol. 53, 504–514. https://doi.org/10.1016/j.jhevol.2007.01.015.
Lepre, C.J., Roche, H., Kent, D.V., Harmand, S., Quinn, R.L., Brugal, J.-P., Texier, P.-J., Lenoble, A., Feibel, C.S., 2011. An earlier origin for the Acheulian. Nature 477, 82–85. https://doi.org/10.1038/nature10372.
Levin, N.E., 2015. Environment and climate of early human evolution. Annu. Rev. Earth Planet. Sci. 43, 405–429. https://doi.org/10.1146/annurev-earth-060614-105310.
Levin, N.E., Brown, F.H., Behrensmeyer, A.K., Bobe, R., Cerling, T.E., 2011. Paleosol carbonates from the Omo Group: Isotopic records of local and regional environmental change in East Africa. Palaeogeogr. Palaeoclimatol. Palaeoecol. 307, 75–89. https://doi.org/10.1016/j.palaeo.2011.04.026.
Li, M., Hinnov, L., Kump, L., 2019. Acycle: time-series analysis software for paleoclimate research and education. Comput. Geosci. 127, 12–22. https://doi.org/10.1016/j.cageo.2019.02.011.
Liddy, H.M., Feakins, S.J., Tierney, J.E., 2016. Cooling and drying in northeast Africa across the Pliocene. Earth Planet. Sci. Lett. 449, 430–438. https://doi.org/10.1016/j.epsl.2016.05.005.
Liu, J., Tian, J., Liu, Z., Herbert, T.D., Fedorov, A.V., Lyle, M., 2019. Eastern equatorial Pacific cold tongue evolution since the late Miocene linked to extratropical climate. Sci. Adv. 5 https://doi.org/10.1126/sciadv.aau6060 eaau6060.
Lupien, R.L., Russell, J.M., Grove, M., Beck, C.C., Feibel, C.S., Cohen, A.S., 2020. Abrupt climate change and its influences on hominin evolution during the early Pleistocene in the Turkana Basin, Kenya. Quat. Sci. Rev. 245, 106531 https://doi.org/10.1016/j.quascirev.2020.106531.
Lupien, R.L., Russell, J.M., Yost, C.L., Kingston, J.D., Deino, A.L., Logan, J., Schuh, A., Cohen, A.S., 2021. Vegetation change in the Baringo Basin, East Africa across the onset of Northern Hemisphere glaciation 3.3–2.6 Ma. Palaeogeography, Palaeoclimatology, Palaeoecology 570, 109426. https://doi.org/10.1016/j.palaeo.2019.109426.
Mana, S., Hemming, S., Kent, D.V., Lepre, C.J., 2019. Temporal and stratigraphic framework for paleoanthropology sites within East-Central Area 130, Koobi Fora, Kenya. Front. Earth Sci. 7, 230. https://doi.org/10.3389/feart.2019.00230.
Martin, J.E., Tacail, T., Braga, J., Cerling, T.E., Balter, V., 2020. Calcium isotopic ecology of Turkana Basin hominins. Nat. Commun. 11, 3587. https://doi.org/10.1038/s41467-020-17427-7.
Maslin, M.A., Trauth, M.H., 2009. Plio-Pleistocene East African pulsed climate variability and its influence on early human evolution. In: Grine, F.E., Fleagle, J.G., Leakey, R.E. (Eds.), The First Humans – Origin and Early Evolution of the Genus *Homo*, Vertebrate Paleobiology and Paleoanthropology. Springer Netherlands, Dordrecht, pp. 151–158.
Maslin, M.A., Brierley, C.M., Milner, A.M., Shultz, S., Trauth, M.H., Wilson, K.E., 2014. East African climate pulses and early human evolution. Quat. Sci. Rev. 101, 1–17. https://doi.org/10.1016/j.quascirev.2014.06.012.
McDougall, I., 1985. K-Ar and $^{40}Ar/^{39}Ar$ dating of the hominid-bearing Pliocene-Pleistocene sequence at Koobi Fora, Lake Turkana, northern Kenya. Geological Society of America Bulletin 96, 159–175.
McDougall, I., Brown, F.H., Vasconcelos, P.M., Cohen, B.E., Thiede, D.S., Buchanan, M.J., 2012. New single crystal $^{40}Ar/^{39}Ar$ ages improve time scale for deposition of the Omo Group, Omo-Turkana Basin, East Africa. J. Geol. Soc. 169, 213–226. https://doi.org/10.1144/0016-76492010-188.
Mercader, J., Akuku, P., Boivin, N., Bugumba, R., Bushozi, P., Camacho, A., Carter, T., Clarke, S., Cueva-Temprana, A., Durkin, P., Favreau, J., Fella, K., Haberle, S., Hubbard, S., Inwood, J., Itambu, M., Koromo, S., Lee, P., Mohammed, A., Mwambwiga, A., Olesilau, L., Patalano, R., Roberts, P., Rule, S., Saladie, P., Siljedal, G., Soto, M., Umbsaar, J., Petraglia, M., 2021. Earliest Olduvai hominins exploited unstable environments ~ 2 million years ago. Nat. Commun. 12, 3. https://doi.org/10.1038/s41467-020-20176-2.
Meyers, S.R., 2014. Astrochron: An R Package for Astrochronology.
Meyers, S.R., Sageman, B.B., Hinnov, L.A., 2001. Integrated quantitative stratigraphy of the Cenomanian-Turonian bridge creek limestone member using evolutive harmonic analysis and stratigraphic modeling. J. Sediment. Res. 71, 628–644. https://doi.org/10.1306/012401710628.
Mohtadi, M., Prange, M., Schefuß, E., Jennerjahn, T.C., 2017. Late Holocene slowdown of the Indian Ocean Walker circulation. Nat. Commun. 8, 1015. https://doi.org/10.1038/s41467-017-00855-3.
Molnar, P., Cane, M.A., 2002. El Niño's tropical climate and teleconnections as a blueprint for pre-Ice Age climates. Paleoceanography 17, 1–11. https://doi.org/10.1029/2001PA000663.
Monger, H.C., Cole, D.R., Buck, B.J., Gallegos, R.A., 2009. Scale and the isotopic record of C_4 plants in pedogenic carbonate: from the biome to the rhizosphere. Ecology 90, 1498–1511. https://doi.org/10.1890/08-0670.1.
Nicholson, S.E., 2017. Climate and climatic variability of rainfall over eastern Africa. Rev. Geophys. 55, 590–635. https://doi.org/10.1002/2016RG000544.
Nicholson, S.E., 2018. The ITCZ and the Seasonal Cycle over Equatorial Africa. Bull. Am. Meteorol. Soc. 99, 337–348. https://doi.org/10.1175/BAMS-D-16-0287.1.
Nutz, A., Schuster, M., Boës, X., Rubino, J.-L., 2017. Orbitally-driven evolution of Lake Turkana (Turkana Depression, Kenya, EARS) between 1.95 and 1.72 Ma: a sequence stratigraphy perspective. J. Afr. Earth Sci. 125, 230–243. https://doi.org/10.1016/j.jafrearsci.2016.10.016.
Olsen, P.E., Laskar, J., Kent, D.V., Kinney, S.T., Reynolds, D.J., Sha, J., Whiteside, J.H., 2019. Mapping solar system chaos with the geological Orrery. Proc. Natl. Acad. Sci. 116, 10664–10673. https://doi.org/10.1073/pnas.1813901116.
Paillard, D., Labeyrie, L., Yiou, P., 1996. Macintosh Program performs time-series analysis. EOS Trans. Am. Geophys. Union 77, 379. https://doi.org/10.1029/96EO00259.
Paquette, J., Drapeau, M.S.M., 2021. Environmental comparisons of the Awash Valley, Turkana Basin and lower Omo Valley from upper Miocene to Holocene as assessed from stable carbon and oxygen isotopes of mammalian enamel. Palaeogeogr. Palaeoclimatol. Palaeoecol. 562, 110099 https://doi.org/10.1016/j.palaeo.2020.110099.
Passey, B.H., Levin, N.E., Cerling, T.E., Brown, F.H., Eiler, J.M., 2010. High-temperature environments of human evolution in East Africa based on bond ordering in paleosol carbonates. Proc. Natl. Acad. Sci. 107, 11245–11249. https://doi.org/10.1073/pnas.1001824107.
Patterson, D.B., Braun, D.R., Allen, K., Barr, W.A., Behrensmeyer, A.K., Biernat, M., Lehmann, S.B., Maddox, T., Manthi, F.K., Merritt, S.R., Morris, S.E., O'Brien, K., Reeves, J.S., Wood, B.A., Bobe, R., 2019. Comparative isotopic evidence from East Turkana supports a dietary shift within the genus *Homo*. Nat. Ecol. Evol. 3, 1048–1056. https://doi.org/10.1038/s41559-019-0916-0.
Pobiner, B.L., Rogers, M.J., Monahan, C.M., Harris, J.W.K., 2008. New evidence for hominin carcass processing strategies at 1.5 Ma, Koobi Fora, Kenya. J. Hum. Evol. 55, 103–130. https://doi.org/10.1016/j.jhevol.2008.02.001.
Polissar, P.J., Rose, C., Uno, K.T., Phelps, S.R., deMenocal, P., 2019. Synchronous rise of African C_4 ecosystems 10 million years ago in the absence of aridification. Nat. Geosci. 12, 657–660. https://doi.org/10.1038/s41561-019-0399-2.
Potts, R., 1998. Variability Selection in Hominid Evolution. Evol. Anthropol. 7, 81–96.
Potts, R., Faith, J.T., 2015. Alternating high and low climate variability: the context of natural selection and speciation in Plio-Pleistocene hominin evolution. J. Hum. Evol. 87, 5–20. https://doi.org/10.1016/j.jhevol.2015.06.014.
Quade, J., Levin, N.E., 2013. East African Hominin Paleoecology: Isotopic evidence from Paleosols. In: Sponheimer, M., Lee-Thorp, J.A., Reed, K.E., Ungar, P. (Eds.), Early Hominin Paleoecology. University Press of Colorado, pp. 59–102. https://doi.org/10.5876/9781607322252:c03.
Quade, J., Cerling, T.E., Bowman, J.R., 1989. Development of Asian monsoon revealed by marked ecological shift during the latest Miocene in northern Pakistan. Nature 342, 163–166. https://doi.org/10.1038/342163a0.
Quinn, R.L., Lepre, C.J., 2019. Revisiting the pedogenic carbonate isotopes and paleoenvironmental interpretation of Kanapoi. J. Hum. Evol. 140, 102549 https://doi.org/10.1016/j.jhevol.2018.11.005.
Quinn, R.L., Lepre, C.J., 2021. Contracting eastern African C4 grasslands during the extinction of *Paranthropus boisei*. Sci. Rep. 11, 7164. https://doi.org/10.1038/s41598-021-86642-z.
Quinn, R.L., Lepre, C.J., Wright, J.D., Feibel, C.S., 2007. Paleogeographic variations of pedogenic carbonate $\delta^{13}C$ values from Koobi Fora, Kenya: implications for floral compositions of Plio-Pleistocene hominin environments. J. Hum. Evol. 53, 560–573. https://doi.org/10.1016/j.jhevol.2007.01.013.
Quinn, R.L., Lepre, C.J., Feibel, C.S., Wright, J.D., Mortlock, R.A., Harmand, S., Brugal, J.-P., Roche, H., 2013. Pedogenic carbonate stable isotopic evidence for wooded habitat preference of early Pleistocene tool makers in the Turkana Basin. J. Hum. Evol. 65, 65–78. https://doi.org/10.1016/j.jhevol.2013.04.002.
Quinn, R.L., Lewis, J., Brugal, J.-P., Lepre, C.J., Trifonov, A., Harmand, S., 2021. Influences of dietary niche expansion and Pliocene environmental changes on the origins of stone tool making. Palaeogeogr. Palaeoclimatol. Palaeoecol. 562, 110074 https://doi.org/10.1016/j.palaeo.2020.110074.

Ravelo, A.C., 2006. Walker Circulation and global warming: lessons from the geologic past. Oceanography 19, 114–122.
Renaut, R.W., Ashley, G.M., 2002. Sedimentation in Continental Rifts. SEPM (Soc. Sediment. Geol.) Special Publication 73. https://doi.org/10.2110/pec.02.73.
Roche, H., Brugal, J.-P., Delagnes, A., Feibel, C., Harmand, S., Kibunjia, M., Prat, S., Texier, P.-J., 2003. Les sites archéologiques Plio-Pléistocènes de la formation de Nachukui, Ouest-Turkana, Kenya: bilan synthétique 1997–2001. Comptes Rendus Palevol. 2, 663–673. https://doi.org/10.1016/j.crpv.2003.06.001.
Rossignol-Strick, M., Nesteroff, W., Olive, P., Vergnaud-Grazzini, C., 1982. After the deluge: Mediterranean stagnation and sapropel formation. Nature 295, 105–110. https://doi.org/10.1038/295105a0.
Ruggieri, E., 2013. A Bayesian approach to detecting change points in climatic records. Int. J. Climatol. 33, 520–528. https://doi.org/10.1002/joc.3447.
Saji, N., Yamagata, T., 2003. Possible impacts of Indian Ocean Dipole mode events on global climate. Clim. Res. 25, 151–169. https://doi.org/10.3354/cr025151.
Saji, N.H., Goswami, B.N., Vinayachandran, P.N., Yamagata, T., 1999. A dipole mode in the tropical Indian Ocean. Nature 401, 360–363. https://doi.org/10.1038/43854.
Sankaran, M., Hanan, N.P., Scholes, R.J., Ratnam, J., Augustine, D.J., Cade, B.S., Gignoux, J., Higgins, S.I., Le Roux, X., Ludwig, F., Ardo, J., Banyikwa, F., Bronn, A., Bucini, G., Caylor, K.K., Coughenour, M.B., Diouf, A., Ekaya, W., Feral, C.J., February, E.C., Frost, P.G.H., Hiernaux, P., Hrabar, H., Metzger, K.L., Prins, H.H.T., Ringrose, S., Sea, W., Tews, J., Worden, J., Zambatis, N., 2005. Determinants of woody cover in African savannas. Nature 438, 846–849. https://doi.org/10.1038/nature04070.
Schefuß, E., Dupont, L.M., 2020. Multiple drivers of Miocene C_4 ecosystem expansions. Nat. Geosci. 13, 463–464. https://doi.org/10.1038/s41561-020-0590-5.
Schrenk, F., Bromaget, T.G., Betzlert, C.G., Ring, U., 1993. Oldest *Homo* and Pliocene Biogeography of the Malawi Rift. Nature 365, 833–836. Macmillan.
Scroxton, N., Bonham, S.G., Rickaby, R.E.M., Lawrence, S.H.F., Hermoso, M., Haywood, A.M., 2011. Persistent El Niño-Southern Oscillation variation during the Pliocene Epoch. Paleoceanography 26, 1–13. https://doi.org/10.1029/2010PA002097.
Semaw, S., Renne, P., Harris, J.W.K., Feibel, C.S., Bernor, R.L., Fesseha, N., Mowbray, K., 1997. 2.5-million-year-old stone tools from Gona, Ethiopia. Nature 385, 333–336. https://doi.org/10.1038/385333a0.
Shanahan, T.M., McKay, N.P., Hughen, K.A., Overpeck, J.T., Otto-Bliesner, B., Heil, C.W., King, J., Scholz, C.A., Peck, J., 2015. The time-transgressive termination of the African Humid Period. Nat. Geosci. 8, 140–144. https://doi.org/10.1038/ngeo2329.
Spoor, F., Leakey, M.G., Gathogo, P.N., Brown, F.H., Antón, S.C., McDougall, I., Kiarie, C., Manthi, F.K., Leakey, L.N., 2007. Implications of new early *Homo* fossils from Ileret, east of Lake Turkana, Kenya. Nature 448, 688–691. https://doi.org/10.1038/nature05986.
Srivastava, P., 2001. Paleoclimatic implications of pedogenic carbonates in Holocene soils of the Gangetic Plains, India. Palaeogeogr. Palaeoclimatol. Palaeoecol. 172, 207–222. https://doi.org/10.1016/S0031-0182(01)00276-0.
Thomson, D.J., 1982. Spectrum Estimation and Harmonic Analysis. Proc. IEEE 70, 1055–1096. https://doi.org/10.1109/PROC.1982.12433.
Tierney, J.E., Ummenhofer, C.C., deMenocal, P.B., 2015. Past and future rainfall in the Horn of Africa. Sci. Adv. 1, e1500682 https://doi.org/10.1126/sciadv.1500682.
Tierney, J.E., Haywood, A.M., Feng, R., Bhattacharya, T., Otto-Bliesner, B.L., 2019. Pliocene Warmth consistent with greenhouse gas forcing. Geophys. Res. Lett. 46, 9136–9144. https://doi.org/10.1029/2019GL083802.
Toth, N., Schick, K., 2019. Why did the Acheulean happen? Experimental studies into the manufacture and function of Acheulean artifacts. L'Anthropologie 123, 724–768. https://doi.org/10.1016/j.anthro.2017.10.008.
Trauth, M.H., Larrasoaña, J.C., Mudelsee, M., 2009. Trends, rhythms and events in Plio-Pleistocene African climate. Quat. Sci. Rev. 28, 399–411. https://doi.org/10.1016/j.quascirev.2008.11.003.
Trauth, M.H., Asrat, A., Berner, N., Bibi, F., Foerster, V., Grove, M., Kaboth-Bahr, S., Maslin, M.A., Mudelsee, M., Schäbitz, F., 2021. Northern Hemisphere Glaciation, African climate and human evolution. Quat. Sci. Rev. 268, 107095 https://doi.org/10.1016/j.quascirev.2021.107095.
Uno, K.T., Polissar, P.J., Jackson, K.E., deMenocal, P.B., 2016. Neogene biomarker record of vegetation change in eastern Africa. Proc. Natl. Acad. Sci. 113, 6355–6363. https://doi.org/10.1073/pnas.1521267113.
Walker, A., Leakey, R.E., Harris, J.M., Brown, F.H., 1986. 2.5-Myr *Australopithecus boisei* from west of Lake Turkana, Kenya. Nature 322, 517–522. https://doi.org/10.1038/322517a0.
Wara, M.W., Ravelo, A.C., Delaney, M.L., 2005. Permanent El Niño-like conditions during the Pliocene warm period. Science 309, 758–761. https://doi.org/10.1126/science.1112596.
Ward, C.V., Leakey, M.G., Brown, B., Brown, F., Harris, J., Walker, A., 1999. South Turkwel: a new Pliocene hominid site in Kenya. J. Hum. Evol. 36, 69–95. https://doi.org/10.1006/jhev.1998.0262.
Weedon, G.P., 2003. Time-series analysis and cyclostratigraphy: examining stratigraphic records of environmental cycles. Cambridge University Press.
White, S.M., Ravelo, A.C., 2020. Dampened El Niño in the early Pliocene warm period. Geophys. Res. Lett. 47 https://doi.org/10.1029/2019GL085504.
White, T.D., WoldeGabriel, G., Asfaw, B., Ambrose, S., Beyene, Y., Bernor, R.L., Boisserie, J.-R., Currie, B., Gilbert, H., Haile-Selassie, Y., Hart, W.K., Hlusko, L.J., Howell, F.C., Kono, R.T., Lehmann, T., Louchart, A., Lovejoy, C.O., Renne, P.R., Saegusa, H., Vrba, E.S., Wesselman, H., Suwa, G., 2006. Asa Issie, Aramis and the origin of *Australopithecus*. Nature 440, 883–889. https://doi.org/10.1038/nature04629.
Wood, B., Boyle, K., 2016. Hominin taxic diversity: Fact or fantasy? Am. J. Phys. Anthropol. 159, 37–78. https://doi.org/10.1002/ajpa.22902.
Wood, B., Constantino, P., 2007. *Paranthropus boisei*: fifty years of evidence and analysis. Am. J. Phys. Anthropol. 134, 106–132. https://doi.org/10.1002/ajpa.20732.
Wood, B., Leakey, M., 2011. The Omo-Turkana Basin Fossil Hominins and their contribution to our understanding of human evolution in Africa. Evol. Anthropol. 20, 264–292. https://doi.org/10.1002/evan.20335.
Wynn, J.G., 2000. Paleosols, stable carbon isotopes, and paleoenvironmental interpretation of Kanapoi, Northern Kenya. J. Hum. Evol. 39, 411–432. https://doi.org/10.1006/jhev.2000.0431.
Wynn, J.G., 2004. Influence of Plio-Pleistocene aridification on human evolution: evidence from paleosols of the Turkana Basin, Kenya. Am. J. Phys. Anthropol. 123, 106–118. https://doi.org/10.1002/ajpa.10317.
Wynn, J.G., Alemseged, Z., Bobe, R., Grine, F.E., Negash, E.W., Sponheimer, M., 2020. Isotopic evidence for the timing of the dietary shift toward C_4 foods in eastern African *Paranthropus*. Proc. Natl. Acad. Sci. 117, 21978–21984. https://doi.org/10.1073/pnas.2006221117.
Yang, W., Seager, R., Cane, M.A., Lyon, B., 2015. The annual cycle of East African precipitation. J. Clim. 28, 2385–2404. https://doi.org/10.1175/JCLI-D-14-00484.1.
Yost, C.L., Lupien, R.L., Beck, C., Feibel, C.S., Archer, S.R., Cohen, A.S., 2021. Orbital influence on precipitation, fire, and grass community composition from 1.87 to 1.38 Ma in the Turkana Basin, Kenya. Front. Earth Sci. 9, 568646 https://doi.org/10.3389/feart.2021.568646.
Zeeden, C., Meyers, S.R., Hilgen, F.J., Lourens, L.J., Laskar, J., 2019. Time scale evaluation and the quantification of obliquity forcing. Quat. Sci. Rev. 209, 100–113. https://doi.org/10.1016/j.quascirev.2019.01.018.
Zhang, Y.G., Pagani, M., Liu, Z., 2014. A 12-Million-year temperature history of the tropical Pacific Ocean. Science 344, 84–87. https://doi.org/10.1126/science.1246172.